2. PHYSICAL CHARACTERISTICS OF THE REGION

This handbook is designed to provide weather analysis and forecast guidance concentrating on the region between latitudes 50 to 60 °N and 150 °W westward to and including the Kamchatka Peninsula. Figure 2-1 shows the region in a larger perspective. The larger perspective is important to consider since many of the storms affecting the Aleutian Islands and Bering Sea region originate far to the southwest near Japan. These storms are further influenced in their movement and intensity changes by the synoptic pattern to the east, from Hawaii (near 20 °N, 155 °W) to the Gulf of Alaska. It is not unusual for a storm center over 1000 n mi (1850 km) away, just east of Japan, to move over the Aleutians and dominate weather conditions in the Bering Sea within a 24- to 36-hr period.

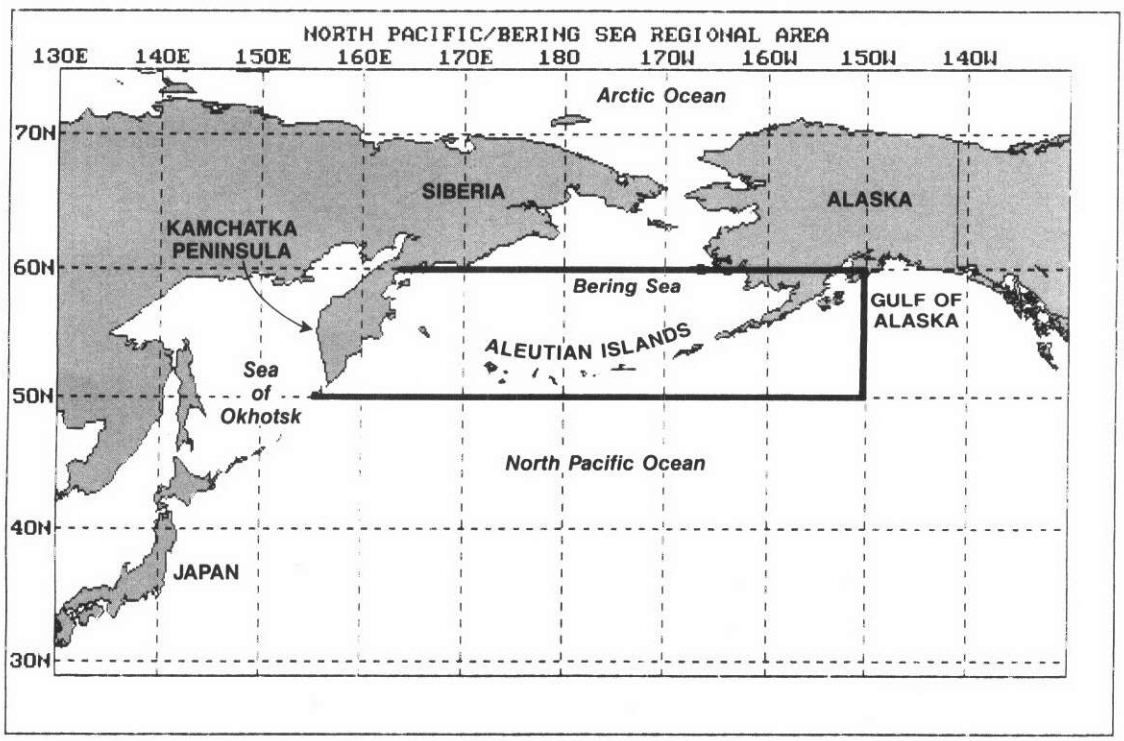

Figure 2-1. Locator chart. North Pacific and Bering Sea regional area.

2.1 Bering Sea and Aleutian Islands

The Aleutian Islands extend 1700 n mi (3150 km) westward from the Alaskan Peninsula in a saucer-shaped pattern. The Aleutian chain approaches within 500 n mi (925 km) of the Kamchatka Peninsula at Attu (near 173 °E), the westernmost island (Fig. 2-2). In so doing the islands separate the Bering Sea to the north from the North Pacific Ocean to the south.

2.1.1 Geography

First discovered by Vitus Bering in 1741, the Aleutian Islands were inhabited by a native population estimated at 25,000. Mass murder and enslavement followed. By 1867, when the Aleutians became part of the United States with the purchase of Alaska, fewer than 2500 native Aleuts remained. This number was further reduced through flu and smallpox epidemics, reaching a low of 1400 at the commencement of World War II.

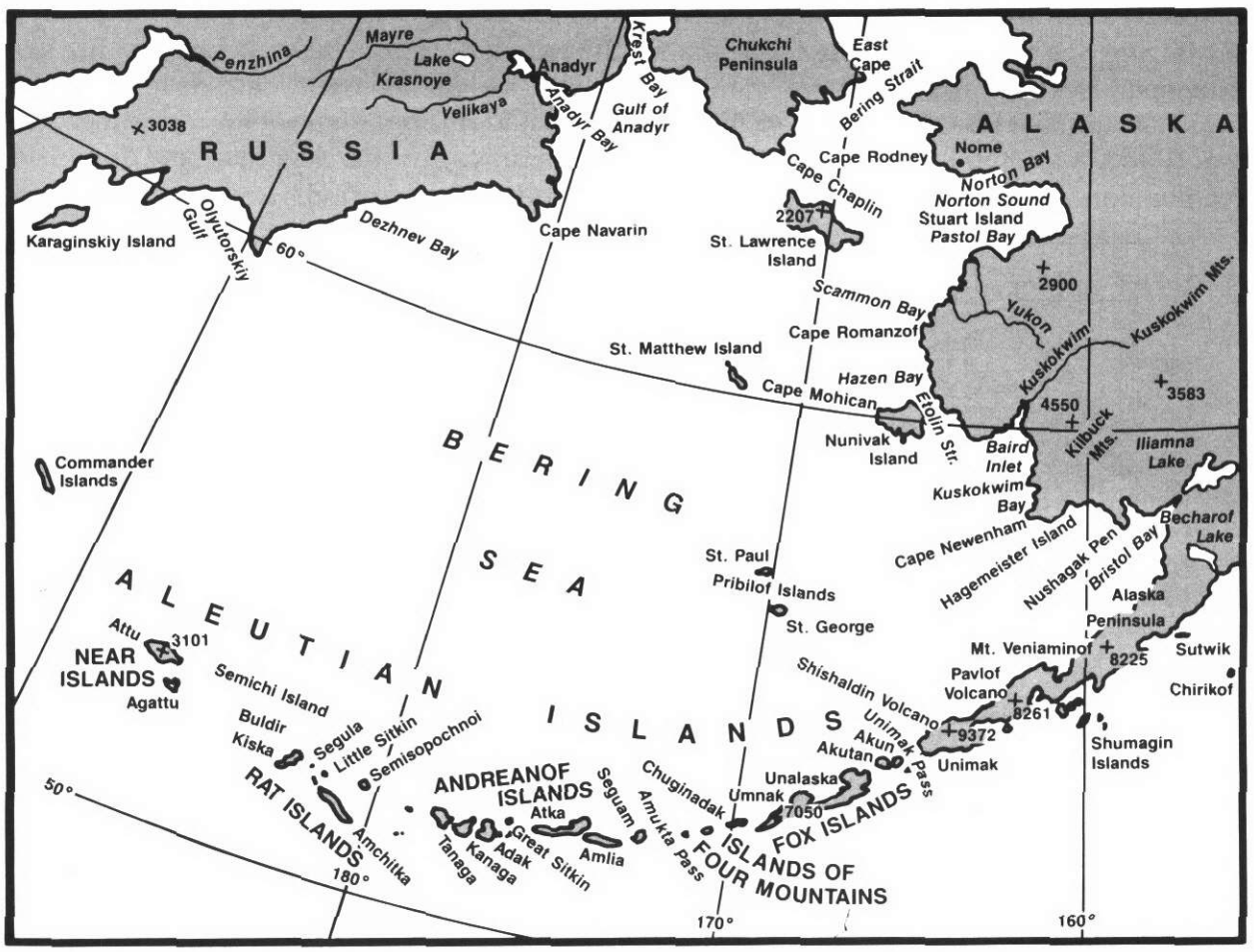

Figure 2-2. Locator chart. Bering Sea and Aleutian Islands.

Military interest in the islands was firmly established by 1940 when the U.S. Navy built a base at Dutch Harbor on Unalaska Island, one of the few good harbors (aside from Adak) in the entire chain. Most of the other islands are surrounded by reefs that make nearby navigation hazardous. The islands are of great strategic interest, made clear on June 3, 1942, when the Japanese bombed Dutch Harbor and followed this with the occupation of Attu and Kiska.

The United States counterattacked, regaining Attu and control of the Aleutians in 1943, and built additional bases on Umnak (169 °W), Atka (174.5 °W), Amchitka (179 °E), and Shemya (Semichi Islands) (174 °E). Shemya Air Force Base and Adak Naval Station remain active today. A Coast Guard station is also active on Kodiak Island. Other bases have converted from military to civilian use over the years.

2.1.2 Topography

The topography of much of the land areas related to this handbook is mountainous and contains some active volcanoes. The ground throughout the Aleutians beyond the Alaskan Peninsula is spongy and marshlike during warm periods and completely frozen during winter. Layers of volcanic ash are usually prevalent below the surface. Very few trees exist except for "Adak National Forest" (a small clump of manually maintained trees). Surface vegetation is abundant, however, and hundreds of varieties of flowers provide a colorful display in summer.

The Fox Islands (Fig. 2-3) extend southwestward starting with Unimak near 164 °W, to Umnak near 169 °W. The Fox Islands received their name from Russian fur traders

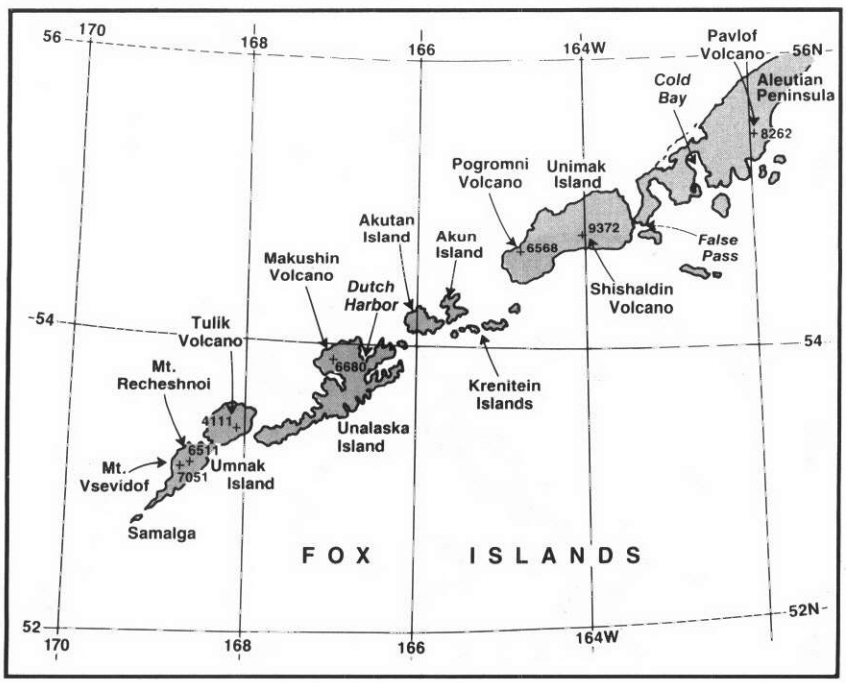

Figure 2-3. Locator chart. Fox Islands.

because of the large fox population of earlier years. The group is distinguished in topography by the highest Aleutian volcano, Shishaldin on Unimak Island, which extends to an elevation of 9372 ft (2857 m). Pogromni volcano (6568 ft or 2002 m) on the southwestern end of the island is another prominent feature. Makushin volcano (6680 ft or 2036 m) is found on Unalaska Island, near Dutch Harbor. Another volcano, Tulik (4111 ft or 1253 m), is found on Uninak, the westernmost island of the Fox group. Mt. Recheshnoi (6511 ft or 1985 m) and Mt. Vsevidof (7051 ft or 2149 m) are also located on Umnak Island.

These topographic features are often apparent in weather satellite images because of their snow-covered domes and high elevation. Figure 2-4 shows a Defense Meteorological Satellite Program (DMSP) infrared example on 8 January 1990 at 0445 GMT. In this image the cold peaks of Veniaminof volcano and Pavlof volcano are clearly visible. Shishaldin volcano is located along a flat east-west oriented ridge that appears as a similarly-oriented narrow white dash in the DMSP image. Gravity waves in the form of "ship wake" patterns are apparent in the region, generated by turbulent effects induced by the topography. The "ship wake" pattern implies a well-mixed lower level with stability maximized at the inversion interface near cloud top level (see NTAG Vol. 1, Sec. 2C).

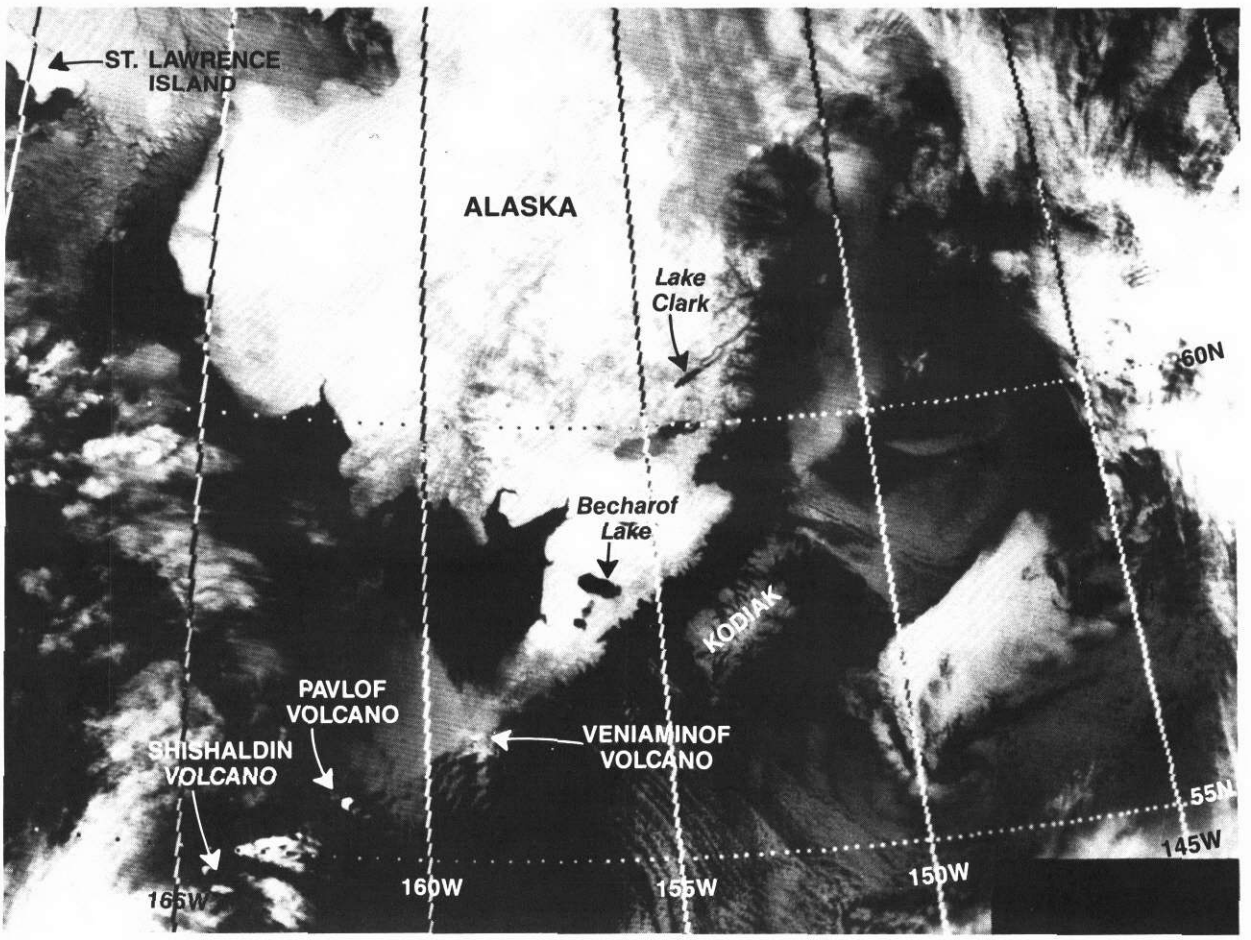

Figure 2-4. DMSP infrared imagery 0445 GMT 8 January 1990.

Figure 2-5 shows the next three groups of islands further west—the islands of the Four Mountains, the Andreanof Islands, and the Delarof Islands. The Islands of the Four Mountains consist of a small group of five islands clustered near 170°W. The tallest of the mountains in this group lies on Chuginadak Island and has an elevation of 5675 ft (1730 m). Yunaska, Chugulak, and Seguam Islands, unnamed as a group, then lead westward to the Andreanof Islands. These islands were explored by a Russian named Andrean Tolstykh in the 1760s and were named after him based on the account he wrote of his explorations. The group includes the island of Adak, present site of a U.S. Navy air strip and port facility (Adak Naval Station). Mount Moffett (3917 ft or 1194 m) is the highest mountain on the island, but mountainous terrain of lesser elevation still acts to provide a blocking action to moderate wind flow from the south. Topography is a key element and influences all forecasts at Adak and, indeed, all locations within the Aleutian chain.

The two final groups of islands in the Aleutian chain are the Rat Islands and the Near Islands. These are shown in Fig. 2-6.

The Rat Islands, so named because of a large rodent population, include Semisopochnoi, Amchitka, Kiska, and Buldir, which lies at the western extremity. Amchitka has a weather service office that provides hourly surface observations and radiosonde data on a routine basis. These observations are monitored very carefully by forecasters at Adak since Amchitka's present weather often becomes Adak's present weather in a matter of a few hours. Problems in applying this concept occur, however, during blocking situations when flow over the Adak-Amchitka area becomes more meridional rather than zonal. In such

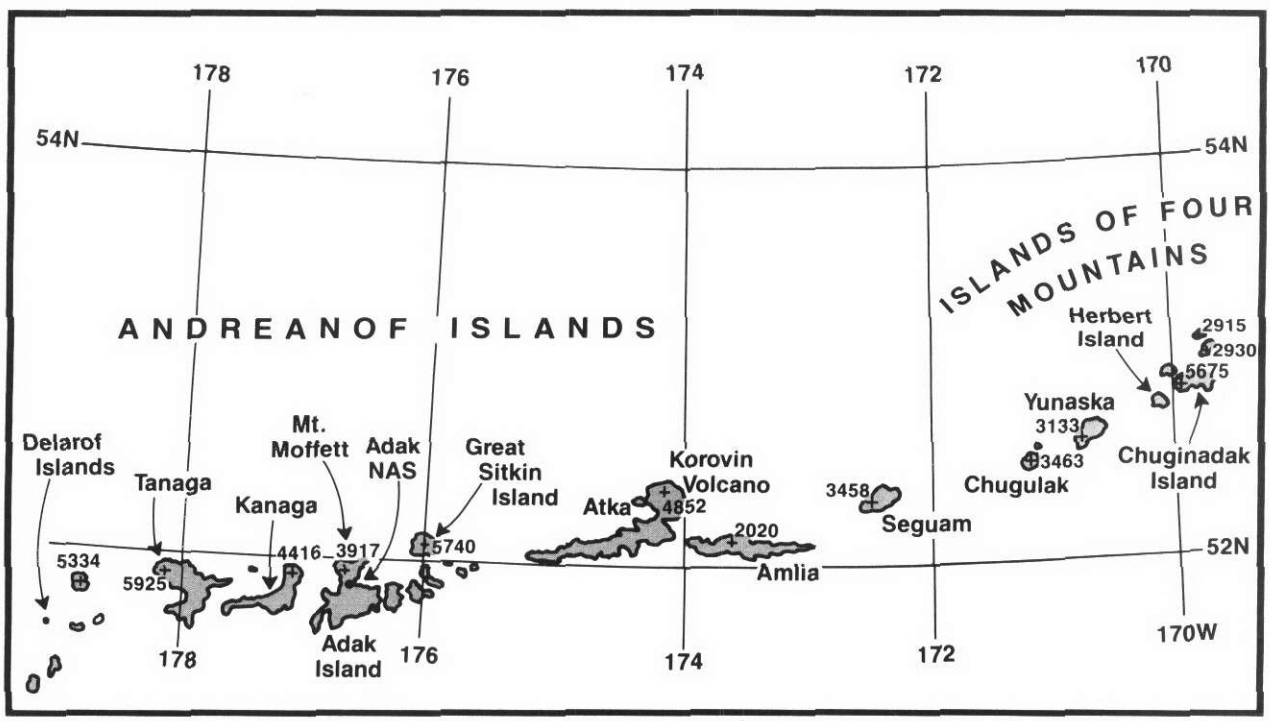

Figure 2-5. Locator chart. Islands of the Four Mountains and Andreanof Islands.

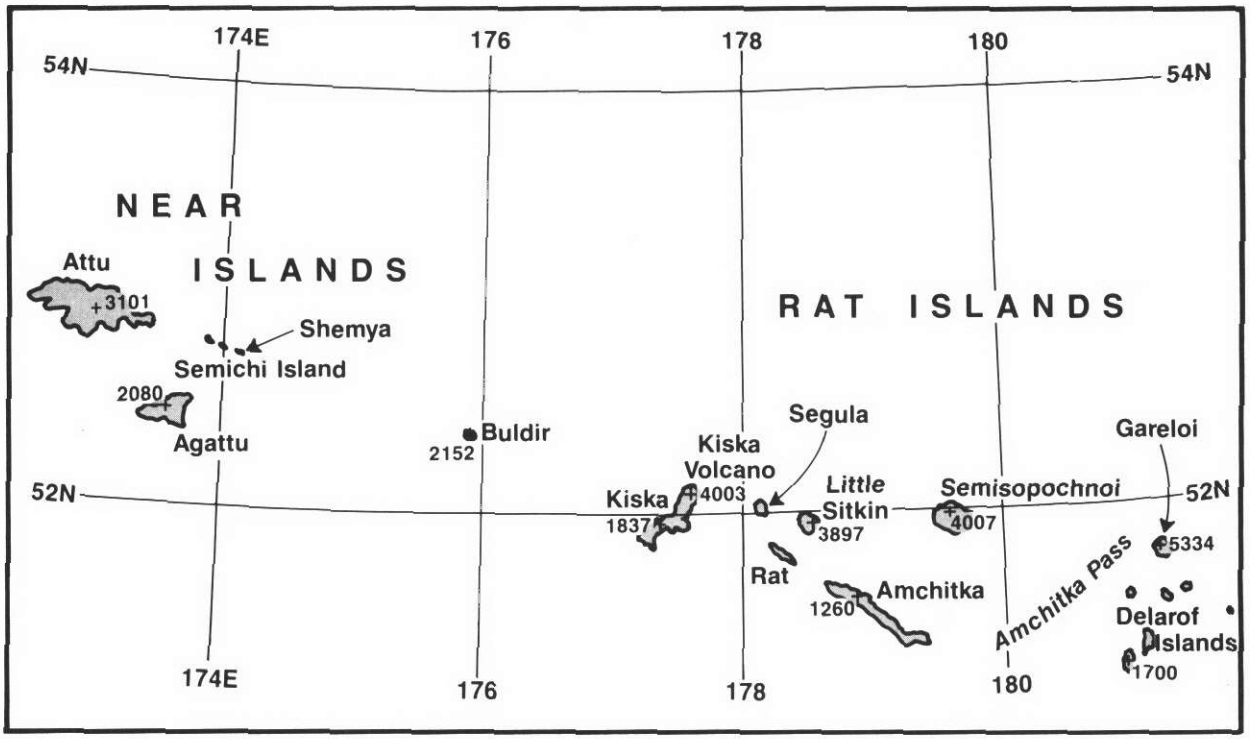

Figure 2-6. Locator chart. Rat Islands and Near Islands.

circumstances the north-south-oriented frontal zone may stall in the region or even slip northward and dissipate. Amchitka's weather and winds at such times cannot be reliably forecast for Adak.

The Kiska volcano (4003 ft or 1220 m) is a prominent topographical feature of the area. Other peaks of about equal height exist on Little Sitkin Island (3897 ft or 1188 m) and on Semisopochnoi Island (4007 ft or 1221 m). Under northerly or southerly flow through the area funneling effects will considerably enhance wind speed in the passages between the mountains, especially when this flow is confined below a strong low-level inversion.

The Near Islands consist of the Semichi group, which includes Attu, Agattu, and Shemya, the site of an U.S. Air Force Base. The group was named because of the relative "nearness" of these islands to the Russian homeland at the time of discovery. The Semichi group is quite flat; however, peaks of 3101 ft (945 m) and 2080 ft (634 m) exist on Attu and Agattu, respectively. The Russian Islands to the west (Commander Islands), although a logical extension of the Aleutian chain, are omitted from this discussion.

2.1.3 Bathymetry

The bathymetry of the Bering Sea and Aleutian Islands region is shown in Fig. 2-7. The Aleutian trench, with depths in excess of approximately 20,000 ft (6000 m), runs parallel to the islands on the south side and continues in its eastward extremity into the northern portion of the Gulf of Alaska. Figure 2-8 shows some of the region's more prominent submarine and physiographic features.

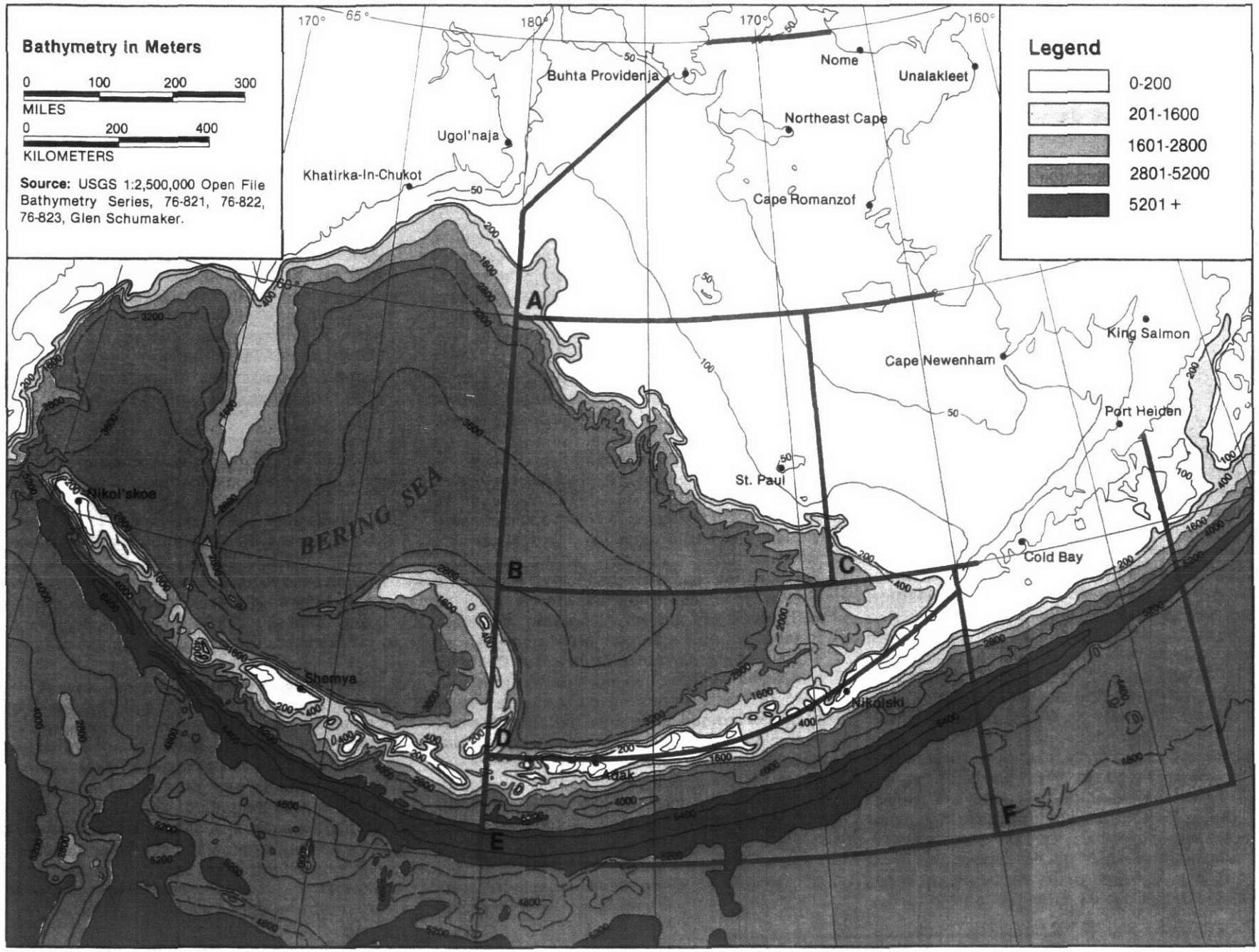

Figure 2-7. Bathymetry of the Bering Sea and Aleutian Island area (Brower et al., 1988).

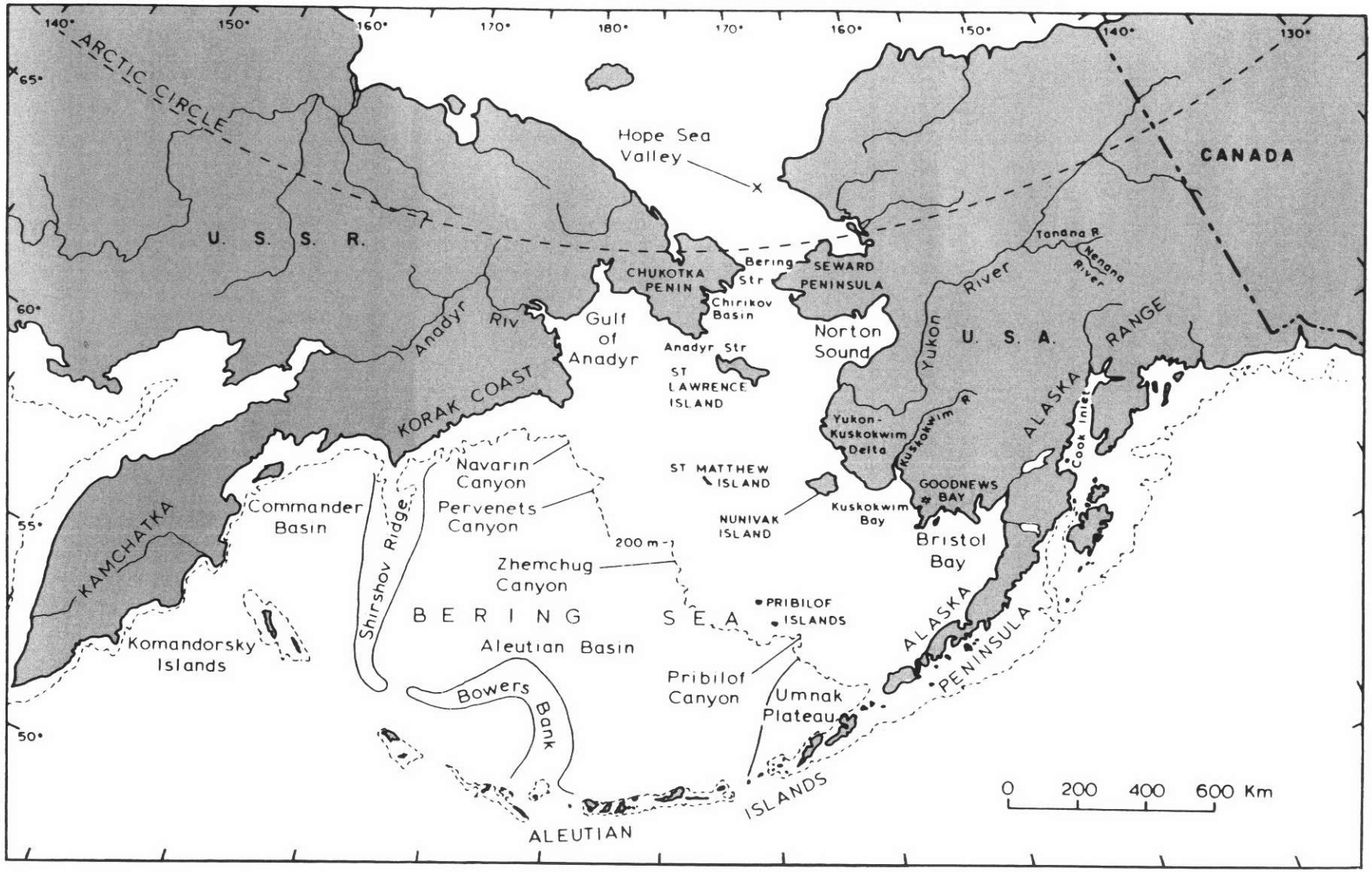

Figure 2-8. Submarine and continental physiographic features of the Bering Sea region (Nelson et al., 1974).

In general, the depth and area of the major openings in the Aleutian-Commander island chain are not large. Of the 39 openings in this chain only 14 have an area greater than 0.3 n mi² (1 km²) and a sill depth of at least 655 ft (200 m). Table 2-1 provides the statistics of these 14 passes on straits. The water is shallowest from the Alaskan Peninsula westward to Amukta Pass near 170°W (Fig. 2-2). Amchitka Pass near 179°E is the only pass east of 172°E having a water depth exceeding 3280 ft (1000 m).

Figure 2-9 is a schematic showing a vertical section of the island passes and straits. From this schematic one can see that the Commander-Near Island Strait and the Kamchatka Strait are the major deep-water passes of the Aleutian chain.

TABLE 2-1. DEPTH AND AREA OF THE MAJOR OPENINGS IN THE ALEUTIAN-COMMANDER ISLAND CHAIN (FAVORITE, 1974)

General Opening	Pass/Strait	Depth (m)	Area (km²)	
East Aleutian group	Samalga	200	3.9	
	Cuginadak	210	1.0	
	Herbert	275	4.8	
	Yunaska	457	6.6	
	Amukta	430	19.3	
	Seguam	165	2.1	37.7
Central Aleutian group	Tanaga	235	3.6	
	Amchitaka	1155	45.7	49.3
West Aleutian	Kiska	110	6.8	
	Buldir	640	28.0	
	Semichi	105	1.7	36.5
Commander-Near St.	Near	2000	239.0	
	Commander	105	3.5	242.5
Kamchatka Strait		4420		335.3
			Total area	701.3

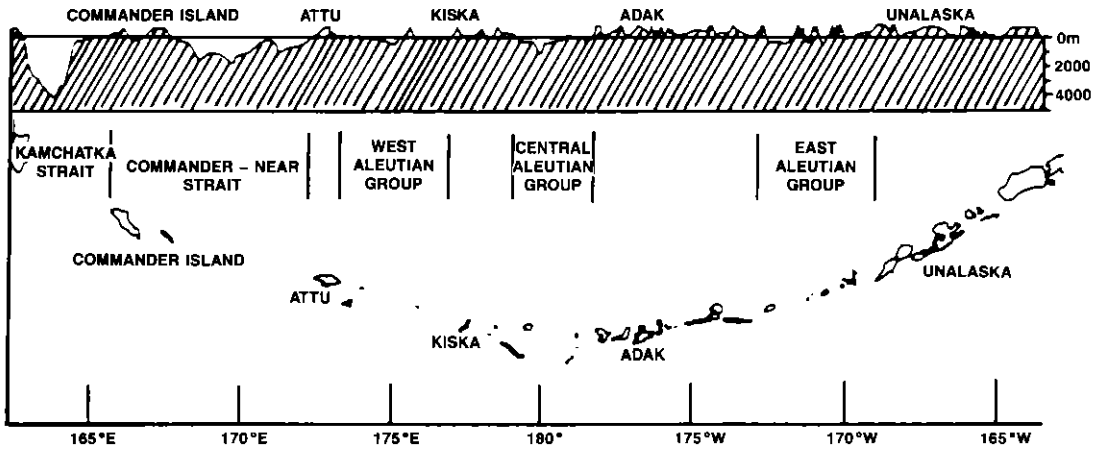

Figure 2-9. Aleutian-Commander island arc and a schematic vertical section of island passes and straits (Favorite, 1974).

2.1.4 Currents

It was originally thought, based on data from the NORPAC (Northern Pacific) Expedition in 1955, that the primary flow of water into the Bering Sea was through Unimak Pass (Fig. 2-2). This source is even suggested in the work by Brower et al. (1988), which provides ocean and atmospheric summaries for the region. However, this viewpoint has been challenged as a physical impossibility since the sill depth for Unimak Pass is only 200 ft or 60 m (Favorite, 1974), which is not of sufficient depth, based on ocean current strength, to permit a large volume of water to enter the region. Actual flow through the various passes in the Aleutian arc is known to be so variable that both north and south flows have been found simultaneously within a single pass.

In such circumstances data are generally inadequate to determine net flow in either direction. The best estimate at the present time is that no net annual exchange occurs through the eastern Aleutian passes, and the westward flowing Alaska Stream provides the major impetus with flow entering the Bering Sea through Amchitka Pass and the Commander-Near Strait. Figure 2-10 shows a diagram of the suggested flow pattern and water mass characterization. Note the clockwise eddies bringing southerly flow through Amchitka Pass near 180° and through the Commander-Near Island pass near 170°E. Major outflow occurs far to the west in the East Kamchatka Current.

The surface circulation pattern is still open to various interpretations because of conflicting results from various data sources. Summer and winter surface circulation patterns are shown in Figs. 2-11 and 2-12, respectively (Brower et al., 1988).

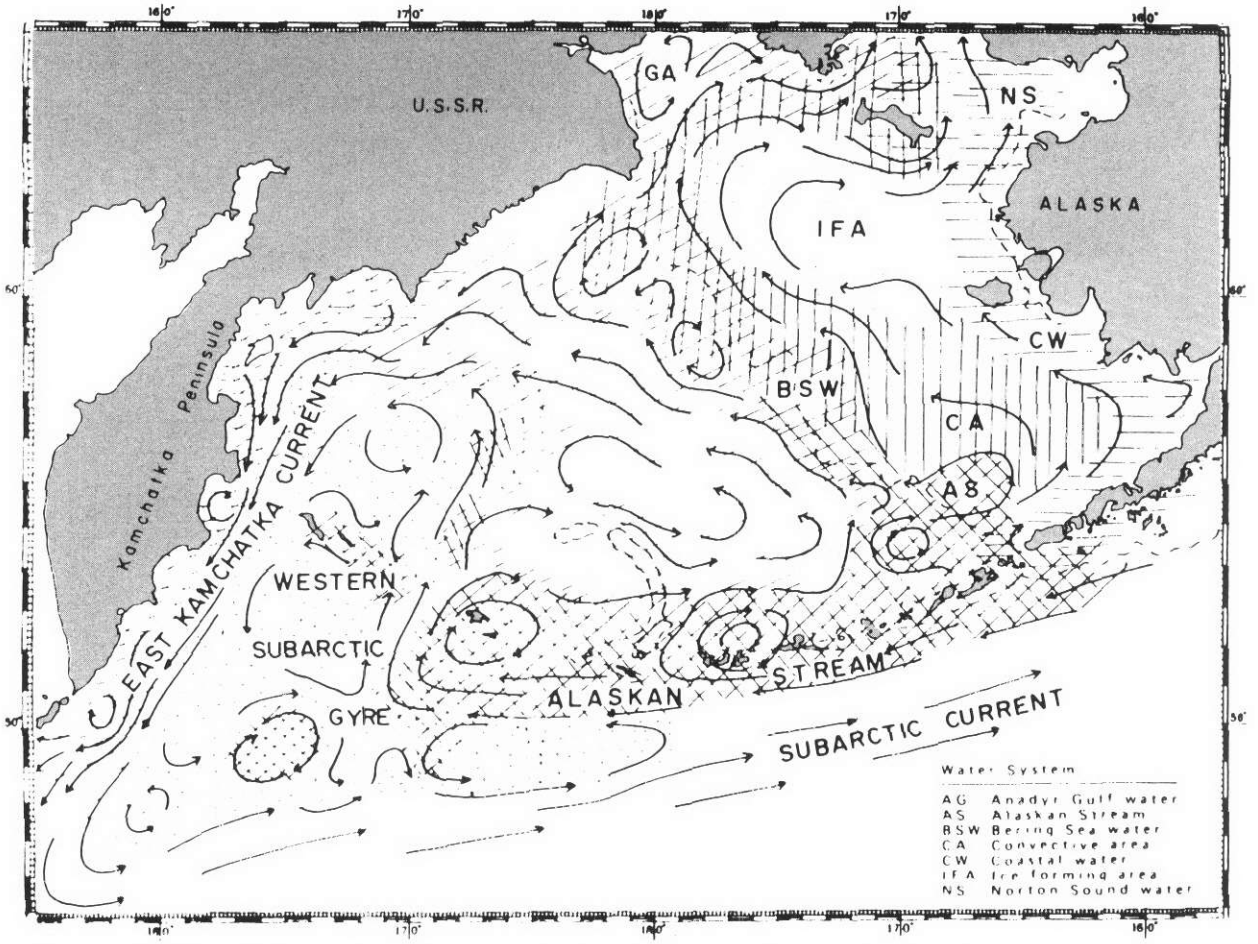

Figure 2-10. Schematic diagram of circulation and extent of water masses in the Bering Sea and northwestern Pacific Ocean (Takenouti and Ohtani, 1974).

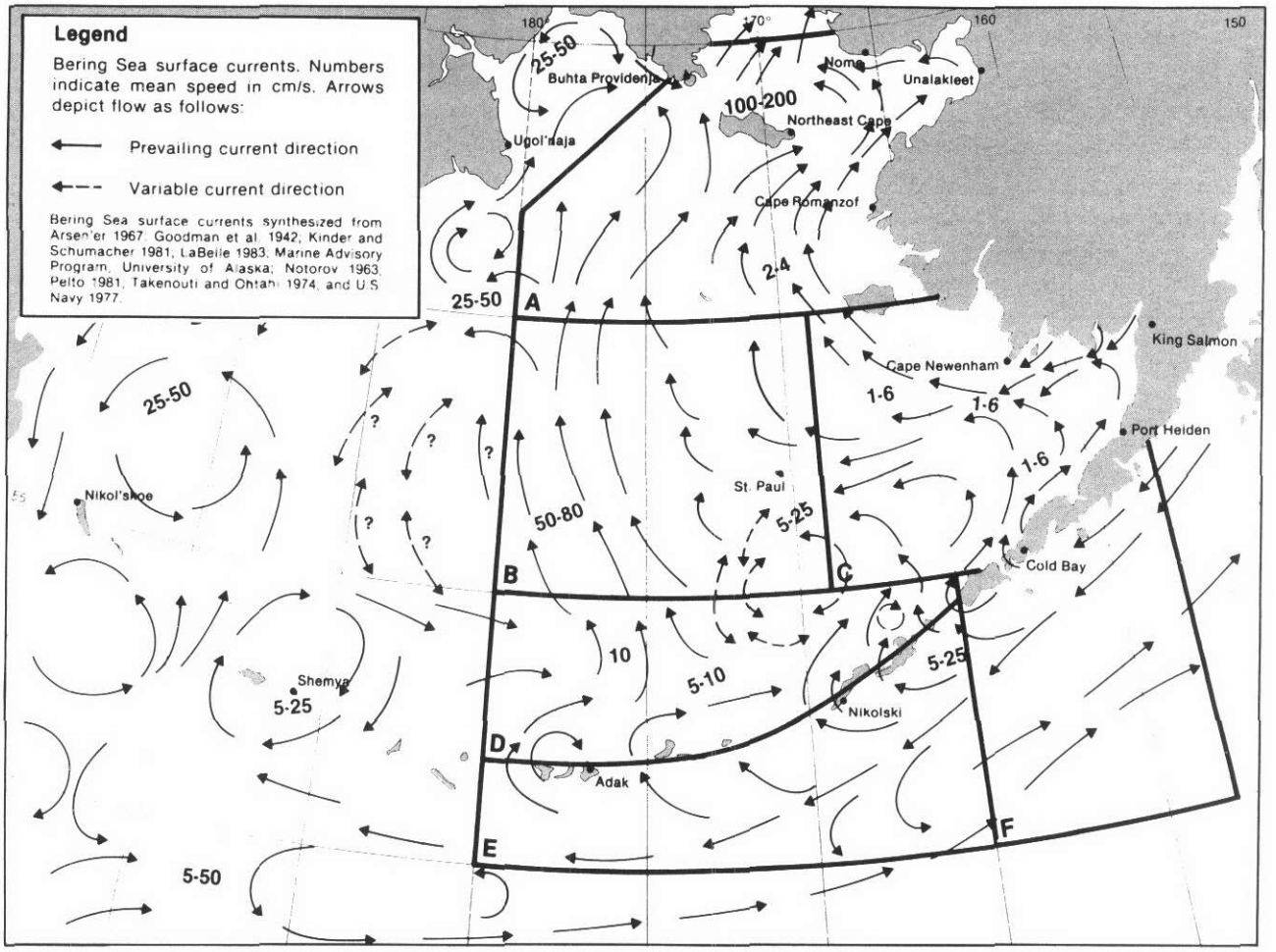

Figure 2-11. Bering Sea currents—summer (Brower et al., 1988).

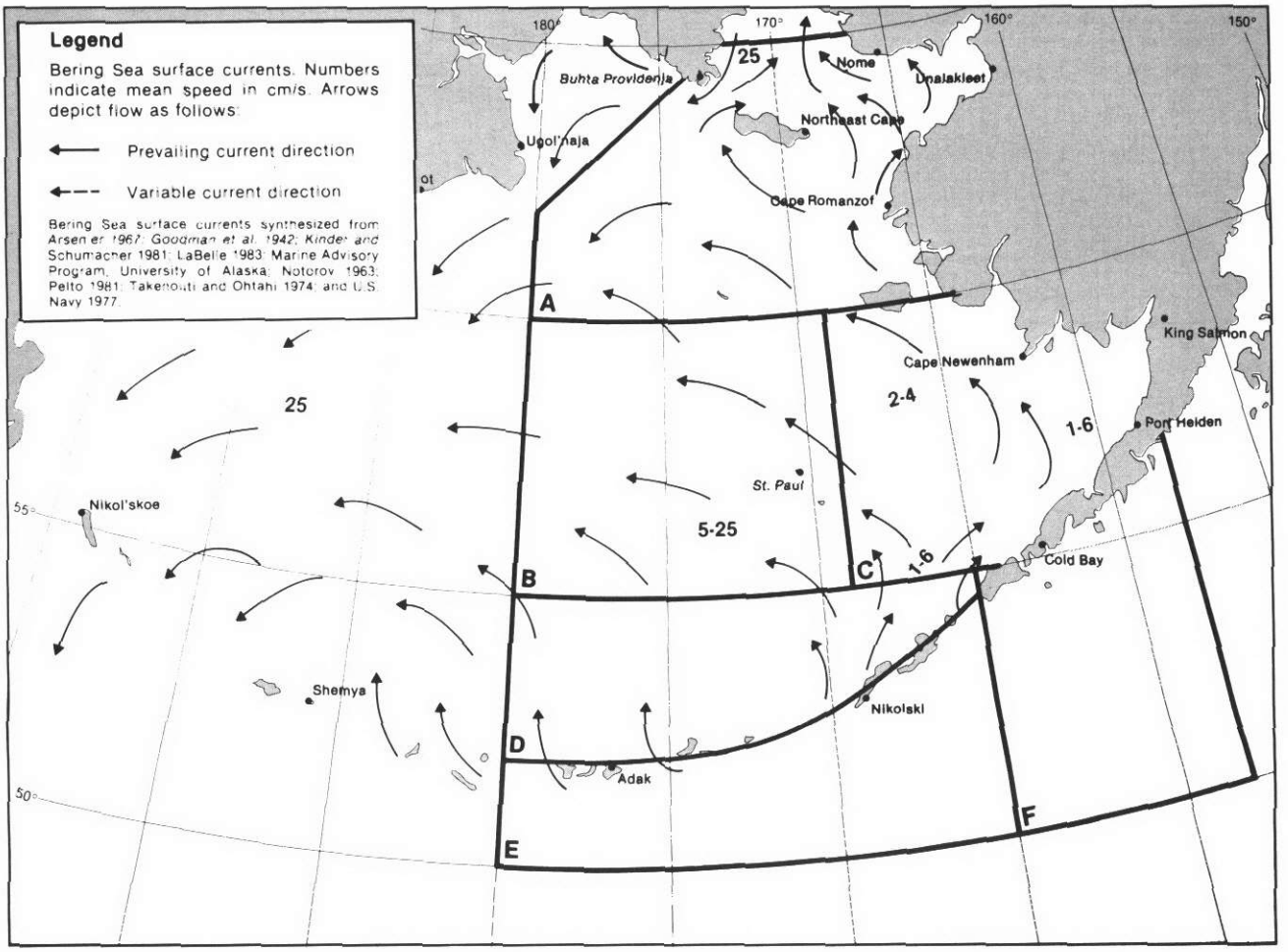

Figure 2-12. Bering Sea currents—winter (Brower et al., 1988).

2.1.5 Tides

The Moon is about twice as effective as the Sun in producing tides. Together they bring about a change in sea level at a given location about every 6 hr. High tide usually occurs twice a lunar day (24 hr, 50 min) at a fixed interval following the Moon's meridional passage. The height difference between high and low tides is called the range of the tide. It is generally greatest during the period of full moon (spring tide) and smallest at half moon or quadrature (neap tide) when the Sun and Moon's overhead longitudes differ by 90°. The range can vary, worldwide, from essentially 0 to over 60 ft (18 m). Figure 2-13 illustrates positioning and tidal effect of the Sun, Moon, and Earth during spring and neap tides. Spring and neap tides occur at approximately 2-week intervals and not seasonally as their names might imply.

Secondary variations include an increase in tidal range when the moon is closest to the Earth (perigee) and a similar decrease when the Moon is furthest from the Earth (apogee).

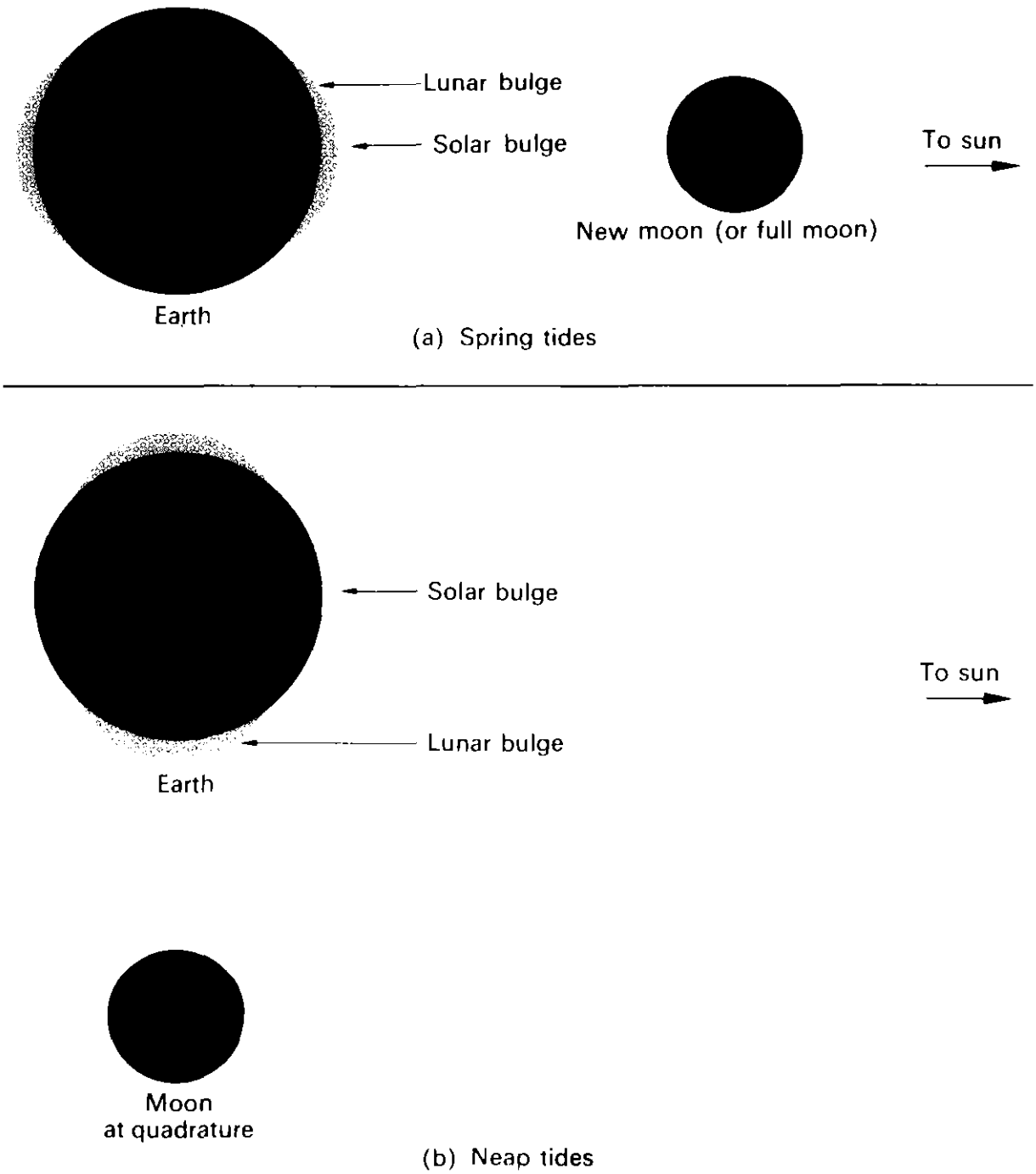

Figure 2-13. (a) Sun, Moon, and Earth aligned to produce spring tides. (b) Sun and Moon acting at right angles to each other to produce neap tides (after Bascom, 1980).

The season of the year also influences the magnitude of high and low water levels with the maximum range occurring at the time of the solstice, during June and December.

A complete discussion of tidal behavior is beyond the scope of the general background material presented here. However, it should be understood that a variety of combinations of forces are involved at any particular time and location, including effects of friction and bottom topography. The complexity of the topic has resulted in defining three types of tides to cover the variations: the semidiurnal tide, the diurnal tide, and the mixed tide. The semidiurnal tide is most common, producing successive high and low tides twice a day about 6 hr apart. The diurnal tide occurs at some locations where only one high tide and one low tide are observed, roughly 12 hr apart. Finally, the mixed tide refers to tides where one of the two maxima is higher than the other. The effect is called diurnal inequality. In this situation a location may experience a high-water level, a highest-high level, a low and a lowest-low level, not in this order of course.

Tidal action in the Bering Sea contains complicated distributions of the three tidal types. Figure 2-14 is a recent assessment of tidal types (Brower et al., 1988) showing the range from high to low tide over the region. Figure 2-15 lists tidal statistics for the Bering Sea at a number of locations. According to Brower et al.:

> "The tide wave enters the Bering Sea as a progressive wave from the North Pacific Ocean, mainly through the central and western passages of the Aleutian-Komandorski Islands (Commander Islands). The Arctic Ocean is a minor secondary source of tides that propagate southward into the north Bering Sea where they complicate the tidal distributions.
>
> Tides in the Bering Sea are considered to be the result of co-oscillation with large oceans. Once inside the Bering Sea, each tidal constituent propagates as a free wave subject to Coriolis effect and bottom friction.
>
> The tide wave propagates rapidly across the deep western basin. Part of it propagates onto the southeast Bering shelf where large amplitudes are found along the Alaska Peninsula and in Kvichak and Kuskokwim Bays (Fig. 2-14). Another part propagates north, eastward past St. Lawrence Island and into Norton Sound. Over most of the eastern Bering shelf region the tide is mainly semi-diurnal, but in Norton Sound diurnal tides predominate. Over the remainder of the Bering tides tend to be mixed. In the Aleutians diurnal rather than semi-diurnal components are stronger."

The influence of the Moon and Sun on ocean tides creates tidal currents of three categories: (a) the rotary type characteristic of currents in the open ocean and along coastal regions; (b) the rectilinear or reversing type, found in inland bodies of water and in bay regions; and (c) the hydraulic type typified by current flow through straits connecting the two independent bodies of water. Tidal currents are much weaker than wind driven currents except in shallow coastal areas. They repeat themselves as regularly as the tidal motions from which they are derived. Tidal currents are strongly influenced by the Coriolis force. For example, in broad estuaries during flood tide in the Northern Hemisphere, the Coriolis force causes a piling up of the water along the shore on one side of the basin during ebbtide.

The Bering Sea is characterized by an open shelf south of St. Lawrence Island. Mean currents are variable in direction and range from 0.02 to 0.08 kt (1 to 4 cm/s), and the

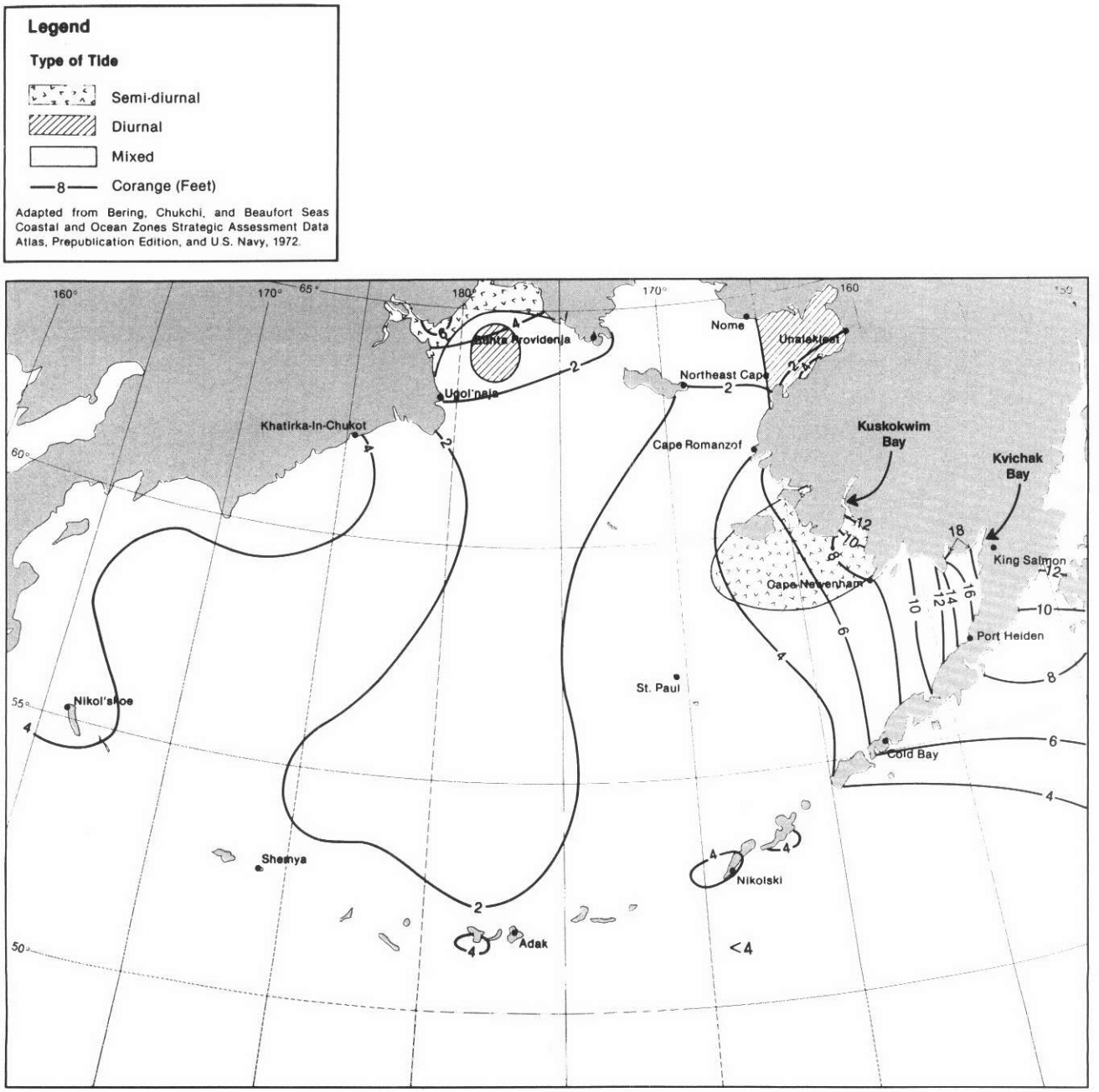

Figure 2-14. Tide types of the Bering Sea (Brower et al., 1988).

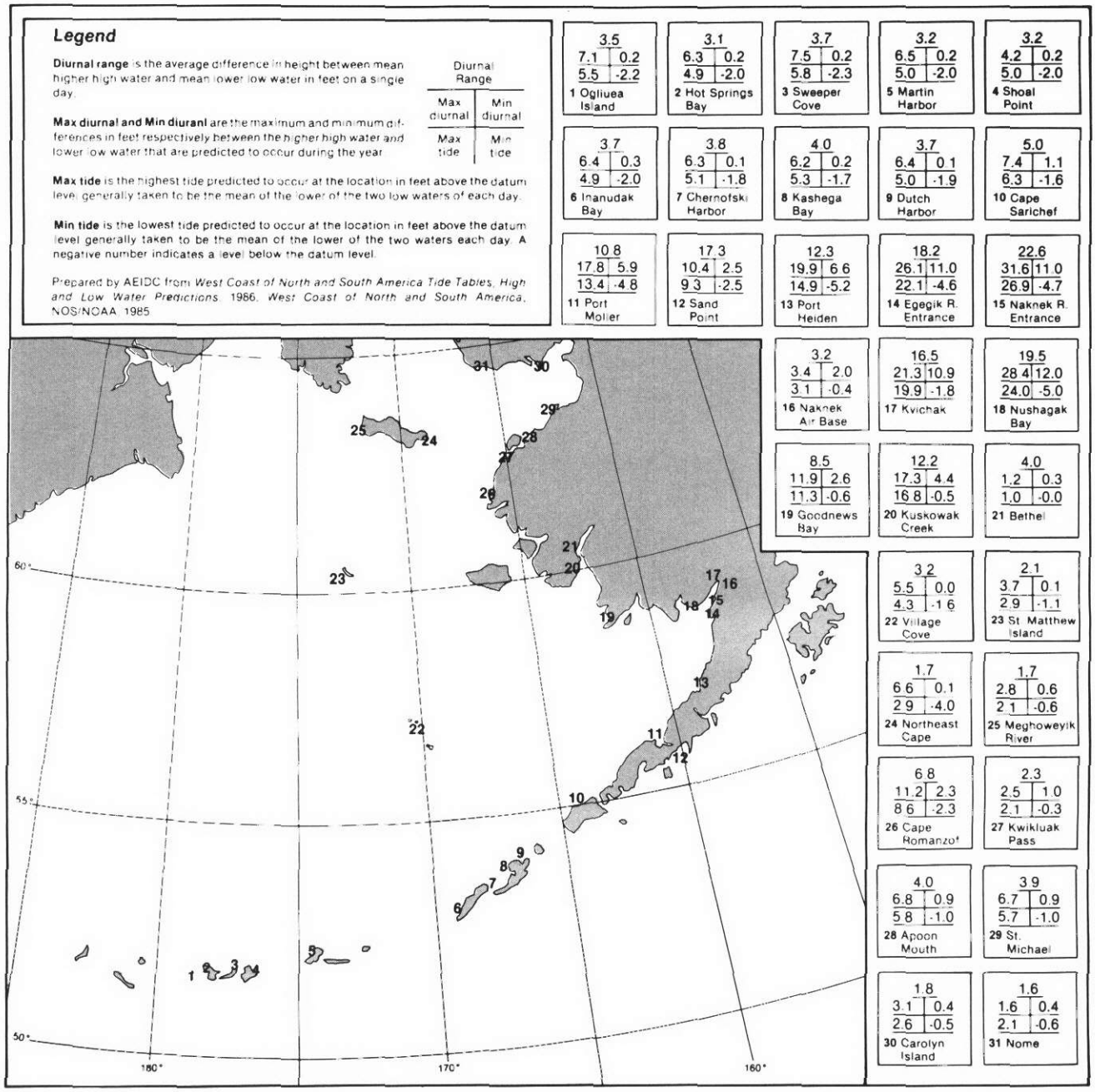

Figure 2-15. Tide statistics for various locations in the Bering Sea (Brower et al., 1988).

tidal current accounts for 55 (± 31)% of the fluctuation (Salo et al., 1983). Near St. Lawrence Island, the Bering Sea narrows into two straits: the Shpanberg to the east and the Anadyr to the west. North of the island the two straits merge to form the Bering Strait. Circulation here is dominated by a northward mean flow ranging from 0.08 to 0.3 kt (4 to 15 cm/s), varying 11% to 37% due to tidal influences (Salo et al., 1983). Flow in both the Anadyr and the Shpanberg is to the north, approximately parallel to the local bathymetry contours. The flow appears to come from around both ends of St. Lawrence Island. Frequent reversals are coincidental with meteorological events. These reversals can affect the flow over vast regions covering thousands of square kilometers. The presence of ice appears to dampen the impact of wind stress forcing. The major driving force for the northward flow through Bering Strait is the sea surface sloping down to the north (Coachman and Aagaard, 1981). The normal condition is one in which sea level in the southern Chukchi Sea (in summer) is about 1.5 ft (0.5 m) lower than in the northern Bering Sea. A major cause of variations in the sea level difference can be traced to fluctuations of the regional wind distribution. It is also possible that the atmospheric pressure field may itself directly modify the oceanic pressure field (Coachman et al., 1975).

2.2 Gulf of Alaska

2.2.1 Geography

The Gulf of Alaska lies between 50 to 60 °N and 130 to 155 °W in the extreme northeast sector of the Pacific Ocean (Fig. 2-16). The region was officially first explored by the Russians in the mid 1700s. Captain Cook, on his third and final voyage sailed from his newly discovered Hawaiian Islands in 1788 to the Pacific Northwest and entered what is now called "Cook's Inlet," leading to Anchorage.

2.2.2 Topography

The Gulf of Alaska is ringed in its northern semicircle by very mountainous terrain. In fact the world's highest coastal range extends from Mount Fairweather (15,310 ft or 4666 m) near Glacier Bay (58.6 °N, 136 °W) to the Chugach Mountains, leading to Prince William Sound, just southeast of Anchorage. Mt. Fairweather has possibly the greatest "sea level to peak" slope of any mountain on Earth. The entire coastal range forms a wall and literally "makes its own weather." The Alaska Range and the Aleutian Range form additional significant barriers. Denali (Mt. McKinley), North America's highest mountain (20,320 ft or 6194 m) is located north of Anchorage in the Alaska Range. Figure 2-17 is a map of the region listing some important places and features.

Heavily wooded mountains are found on the Kenai Peninsula, Afognak Island, Kodiak Island, and on the southeastern portion of the Alaska Peninsula (Fig. 2-18). These mountains provide a block to northwesterly winds that often flow with hurricane force through a gap over Kamishak Bay, then past the Barren Islands, at the entrance to Cook Inlet, and out into the Gulf of Alaska. Low terrain leads from near King Salmon across the Alaskan Peninsula to Kamishak Bay. This gap is referred to as the Kamishak Gap. Gap winds also flow through Shelikof Strait when, with high pressure inland, isobars are aligned parallel to the Shelikof Strait axis. Figure 2-19 is a mesoscale analysis showing aircraft-measured winds at 260 ft (80 m) during such an event. Northerly winds at the strait entrance veered southeasterly a short distance into the strait. It was also noted that wind speed increased through the strait from about 10 kt (5 m/s) at the entrance to 25 kt (13 m/s) near the exit.

The Alaskan Peninsula is typified by a flat tundra region on the northwest side, numerous mountains of the Aleutian Range on the southeast side, and the Pavlof volcano (8262 ft or 2518 m) near 162 °W (Fig. 2-3). The Veniaminof volcano (8225 ft or 2507 m) near 159.5 °W is a dominant feature of the southwest portion of the peninsula. The peninsula terminates just southeast of Cold Bay where a narrow channel (False Pass) separates it from Unimak Island (Fig. 2-3).

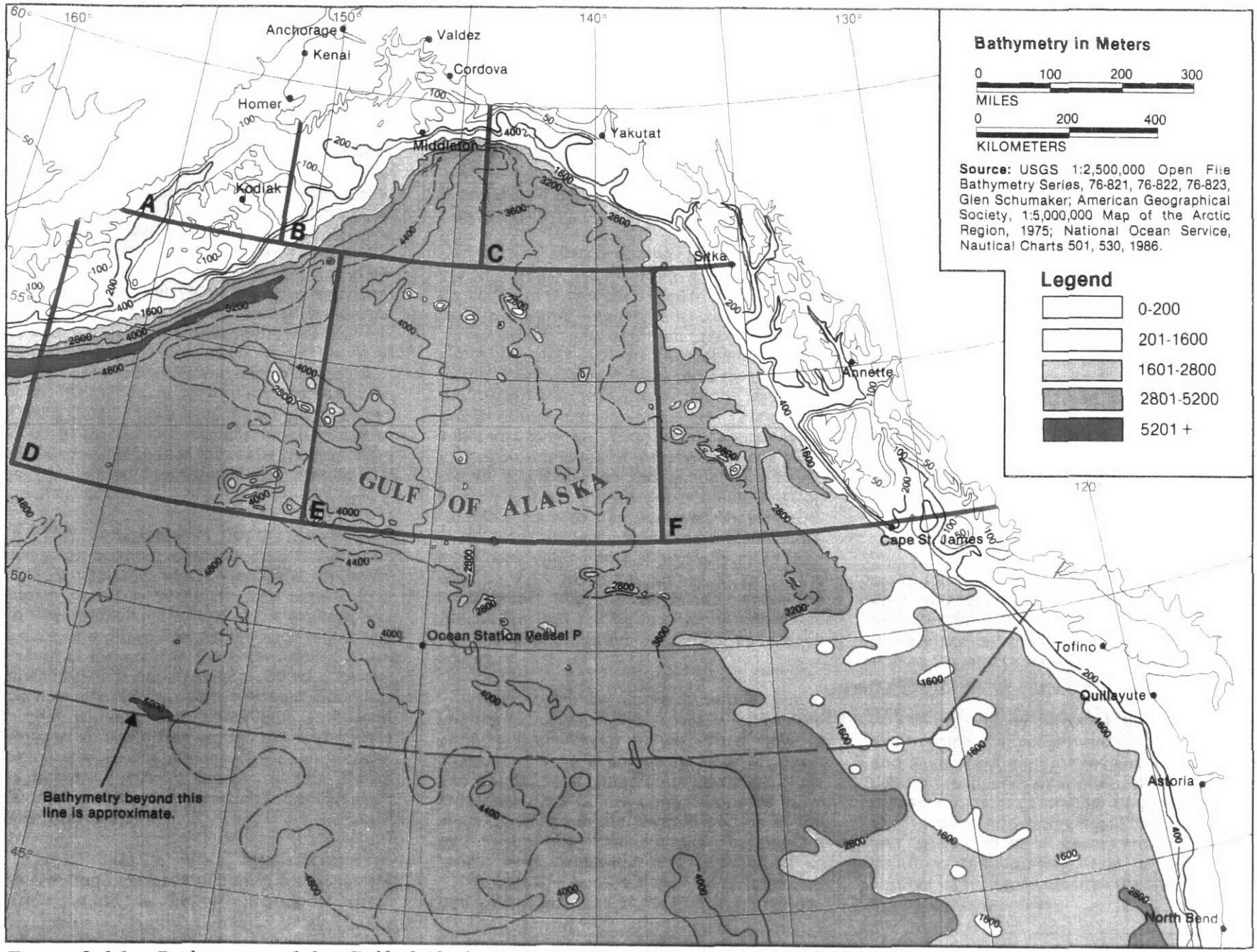

Figure 2-16. Bathymetry of the Gulf of Alaska (adapted from Brower et al., 1988).

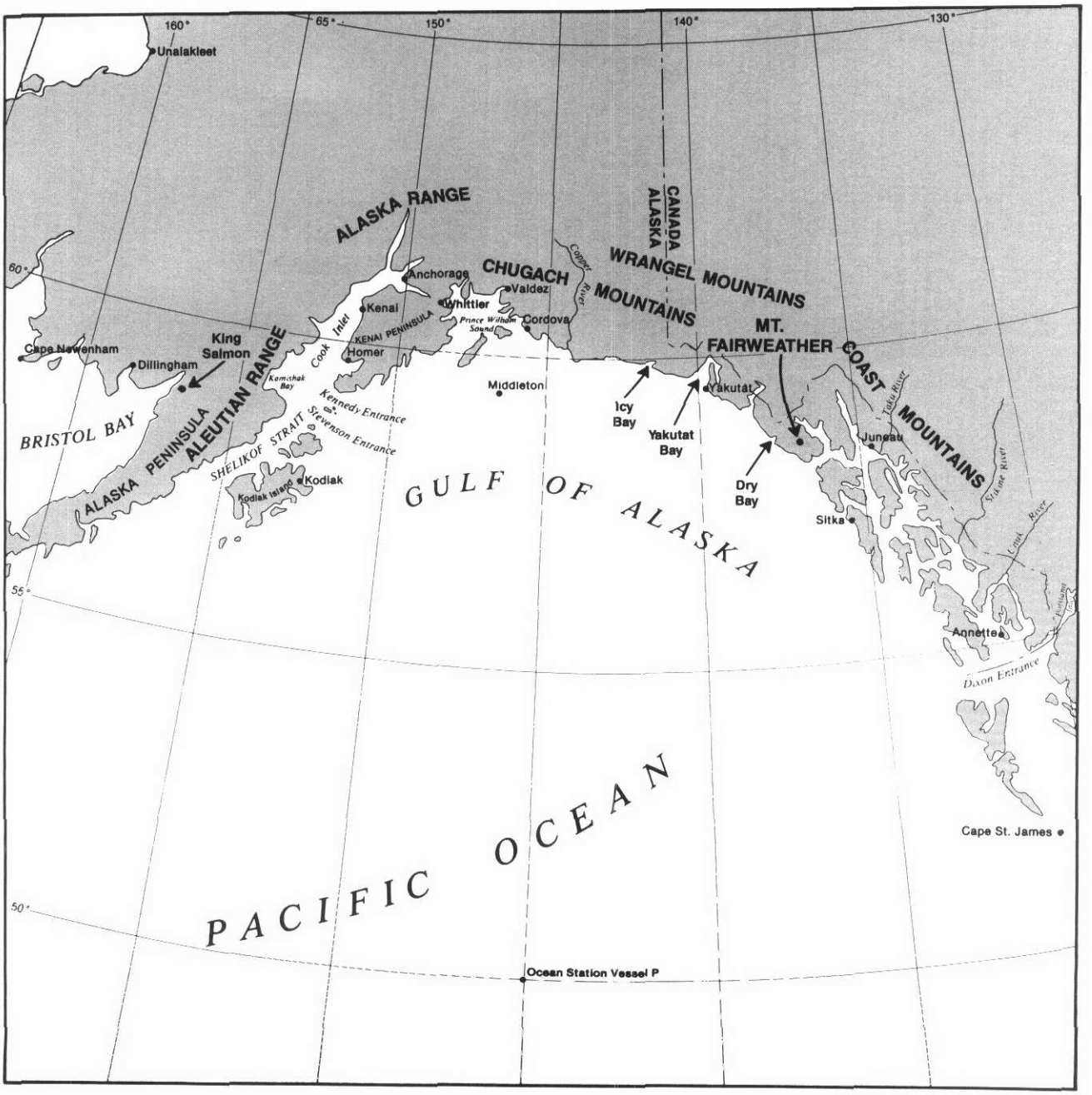

Figure 2-17. Locator map for the Gulf of Alaska (adapted from Brower et al., 1988).

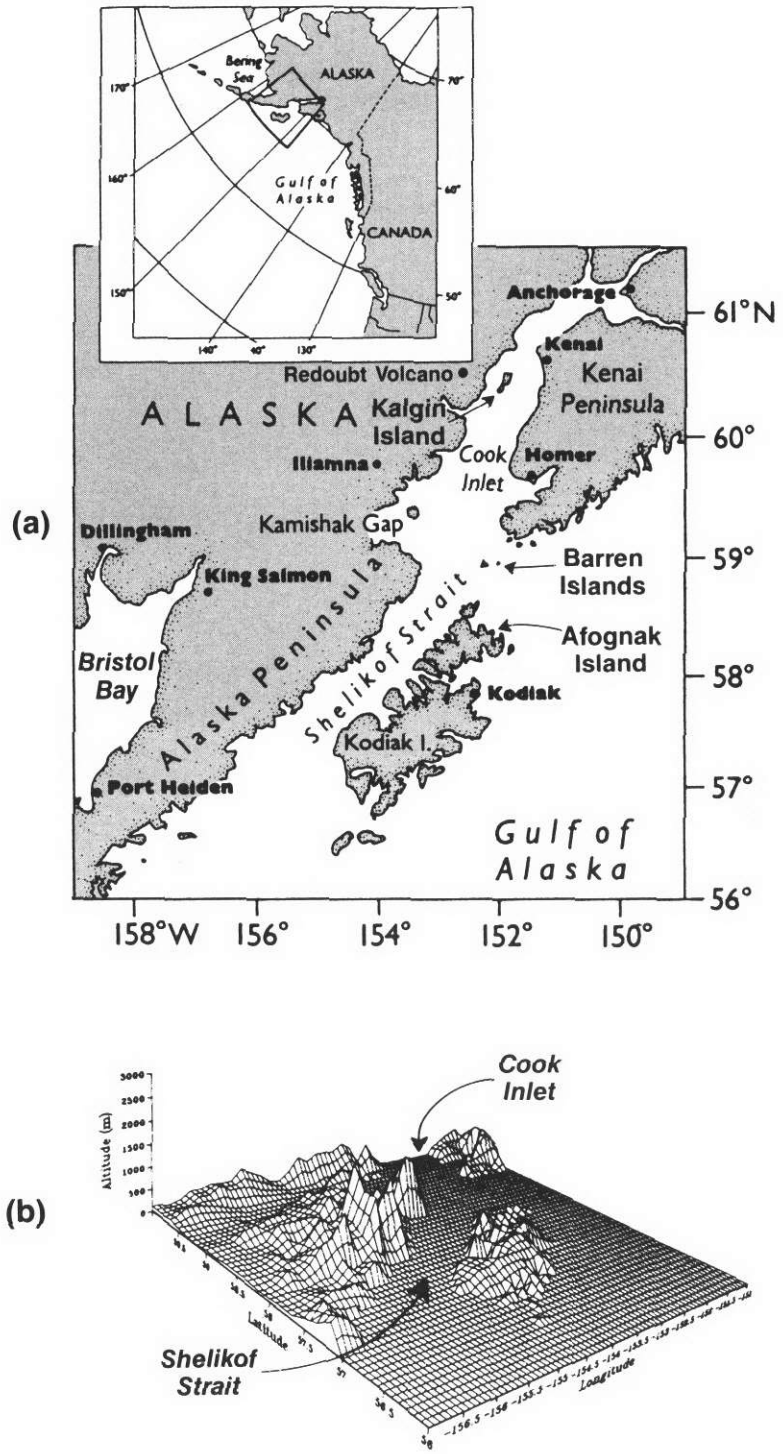

Figure 2-18. *(a) Shelikof Strait region; (b) Topography of the Shelikof Strait region. Horizontal grid spacing is 5 min, vertical scale exaggerated 50 times (adapted from Lackmann and Overland, 1989).*

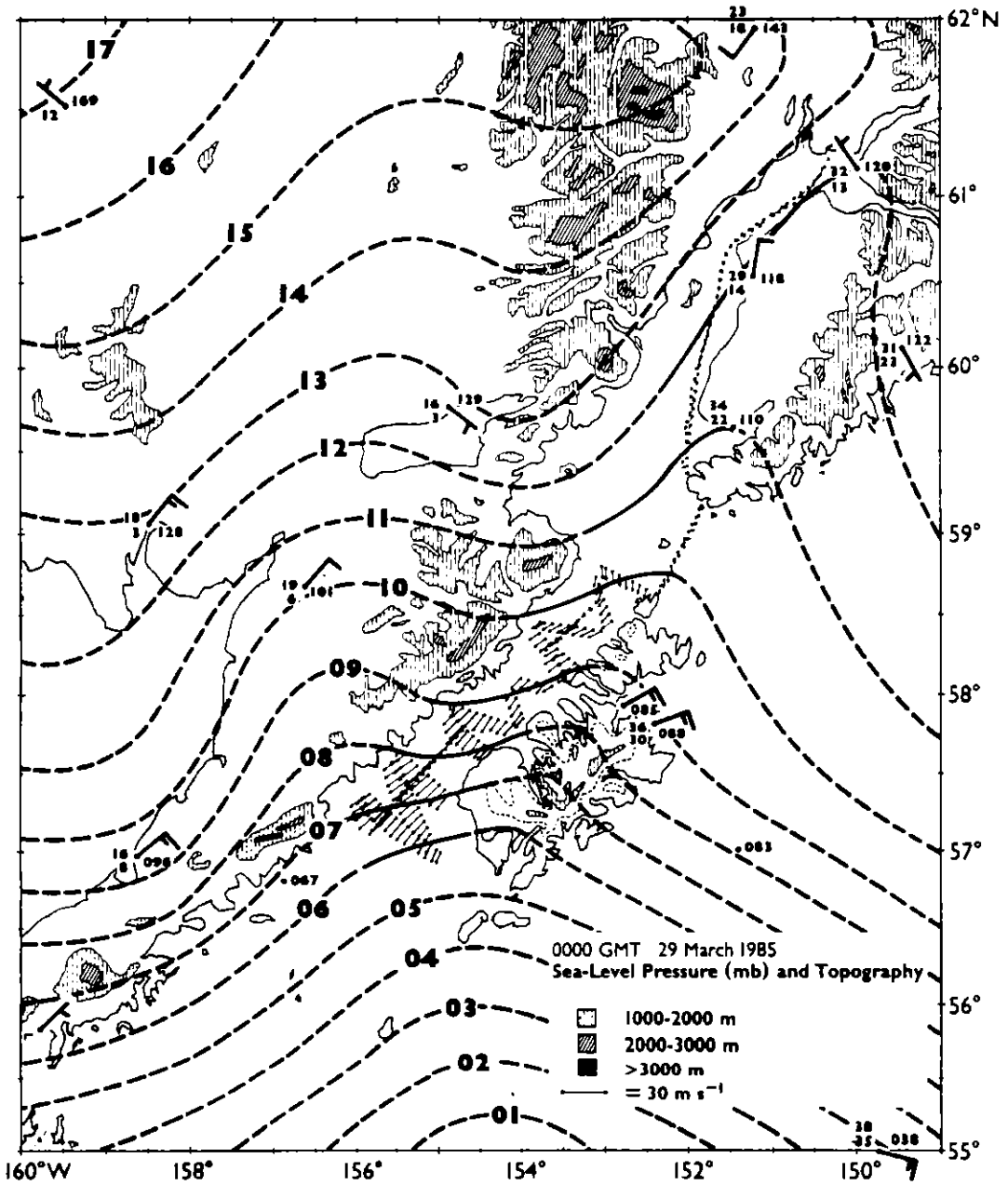

Figure 2-19. Mesoscale sea-level pressure analysis and topography. Isobars are dashed outside of areas where aircraft data were collected and over topography to indicate a higher degree of uncertainty. Station temperatures and dewpoints are in °F, pressures are in mb – 1000 (Lackmann and Overland, 1989).

2.2.3 Bathymetry

The bathymetry of the Gulf of Alaska is shown in Fig. 2-16. It can be seen that the shallowest water is to the southeast, and the deepest water is in the trench that parallels the south side of the entire Aleutian chain and extends eastward to an area just south of Kodiak Island.

2.2.4 Currents

The North Pacific Current, an eastward extension of the Kuroshio Current crosses the ocean near 45 °N. It then splits into two branches offshore of Washington and Oregon. The southward flowing branch is called the California Current and the northward flowing branch, the Alaska Current. In the region of the Gulf of Alaska the system describes a huge cyclonic gyre, centered near 52 °N, 140 to 145 °W during both winter and summer. Figure 2-20 is a depiction of the summer sea surface currents in that area (Brower et al.,

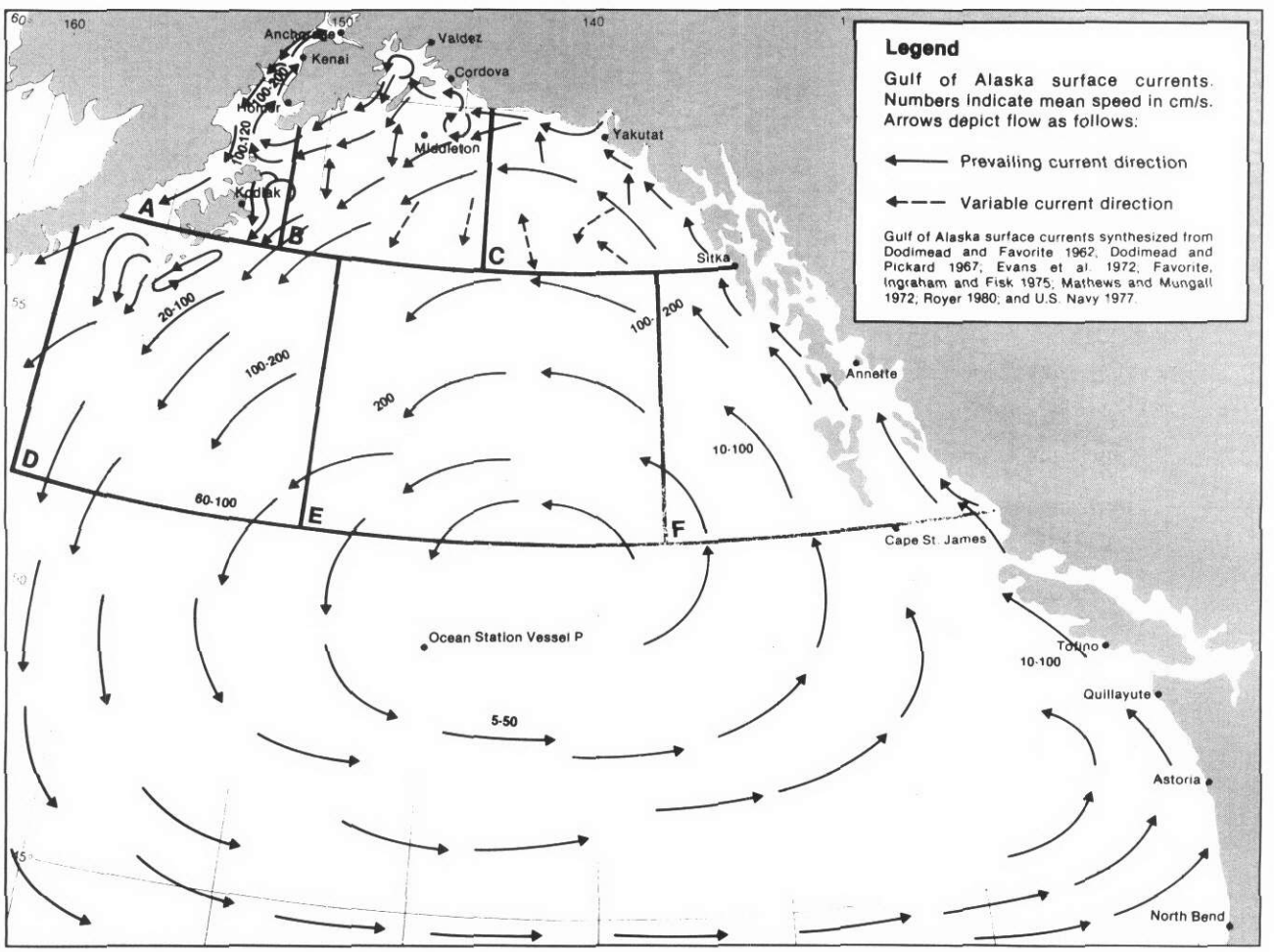

Figure 2-20. Gulf of Alaska sea surface currents: Summer (Brower et al., 1988).

1988). The companion winter pattern is shown in Fig. 2-21. No appreciable seasonal shift is apparent in the position of the current.

The current narrows with maximum speed along the shelf break near Kodiak (Fig. 2-21). In this region the current is referred to as the "Alaska Stream." Maximum current velocities in the region of 4 kt (2 m/s) have been noted.

The circulation near the shelf break contains frequent meanders and eddies, associated with changes in bathymetry (See Section 6 for related case study). Eddy formation is most notable in the fall. The eddies propagate eastward on the north (shoreward) side of the Alaska Current, moving onto the continental shelf with rotational speeds of up to 1 kt (0.5 m/s). Troughs or trenches extend from the shelf break into Yakutat Bay and Icy Bay. In these regions flow is often diverted anticyclonically toward shore in an easterly flow.

A small anticyclonic eddy called the Kayak Island eddy is located just south of Cordova (Fig. 2-20). The eddy circulates in a typical speed of 0.6 kt (0.3 m/s).

The Kenai Current or the Alaska Coastal Current, a narrow intense current associated with fresh water runoff, extends from Prince William Sound through the Shelikof Strait

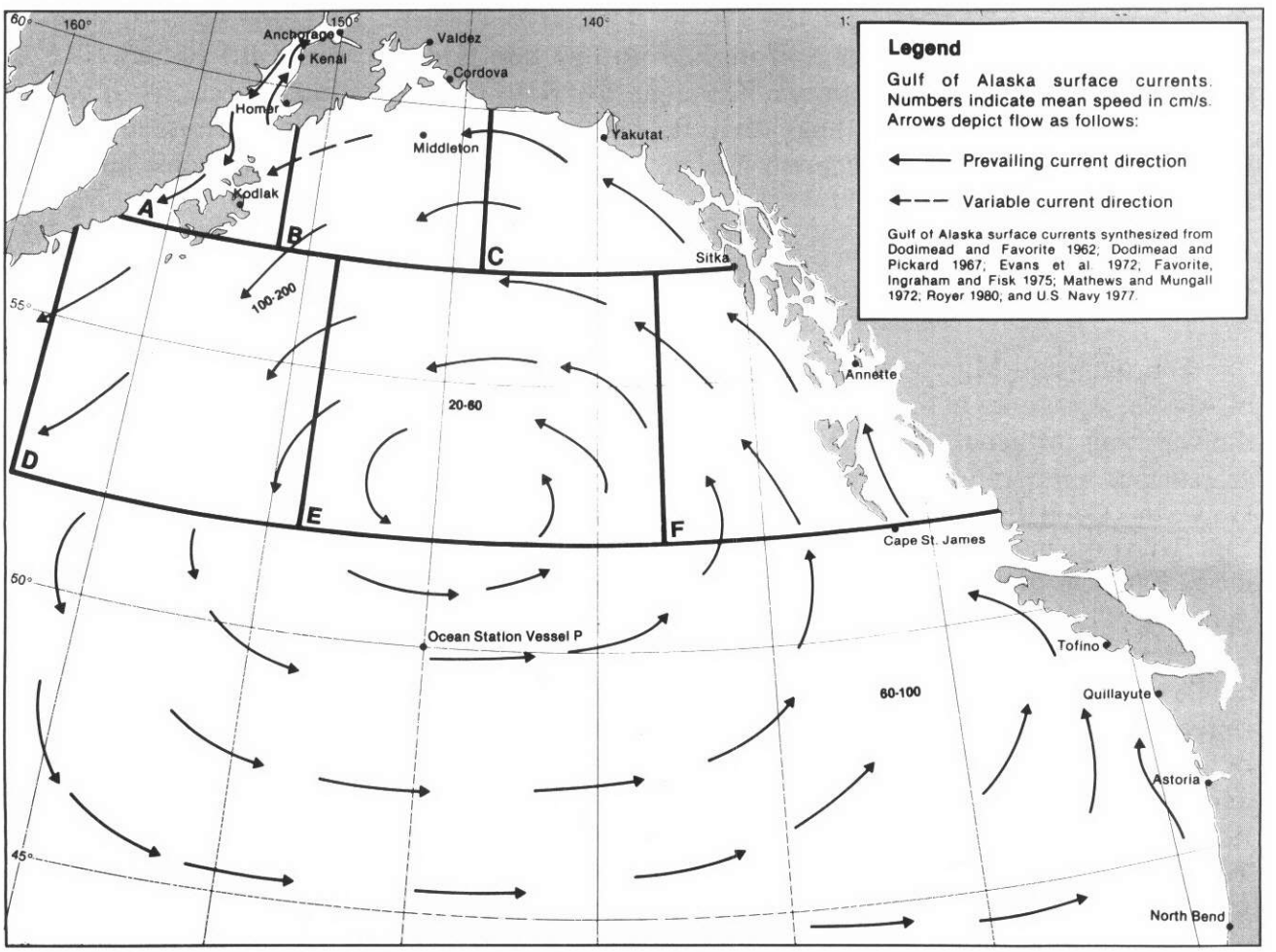

Figure 2-21. Gulf of Alaska sea surface currents: Winter (Brower et al., 1988).

to the western end of the Alaska Peninsula. The current is quite narrow with widths estimated from 2.7 to 13.5 n mi (5–25 km). Speed can be quite high reaching 2 to 3 kt (1–1.5 m/s) in some areas. Maximum speeds are usually noted in mid to late autumn.

Observations have shown that flow entering the Kennedy Entrance (between Barren Islands and Kenai Peninsula) to Cook Inlet is stronger and more persistent than flow entering the Stevenson Entrance (between Kodiak Island and Barren Islands). Speeds of 0.6 kt (0.3 m/s) are commonly observed, being stronger near the Kenai Peninsula. Superimposed on the current speed are tidal speeds reaching 1 kt (>0.5 m/s) in the Kennedy Entrance.

The current flow in Cook Inlet is interesting in that clear oceanic water enters the inlet from the southeast on the south side of the inlet during floodtide and departs as turbid water along the north and west coast during ebbtide. Currents near Kalgin Island, just east of the Redoubt Volcano (Fig. 2-18), are complex. In this region ebbtides and floodtides meet, speeds are higher, and occasional strong cross-inlet currents are observed. Peak velocities of 6 to 8 kt (3–4 m/s) occur during tidal extremes.

2.2.5 Tides

Figure 2-22 shows the range from high to low tide typical of the Gulf region. The tides are of the mixed type with two highs and two lows per day in most locations. It can be seen that a very high tidal range of 30 ft (9 m) is characteristic of the Anchorage area. Secondary maximum tides occur in Nushagak and Kvichak Bay at the northeast end of Bristol Bay.

2.2.6 Sea Ice and Sea Surface Temperature

February and March are typified by the coldest sea surface temperatures in the Gulf of Alaska. A bulging of the isotherms northward along the southeast coast of Alaska reflects the warming influence of the Alaska Current in that region. Figure 2-23 shows the mean sea surface temperature for February. The Gulf of Alaska is ice free throughout the year. However, Cook Inlet has appreciable ice amounts (shown as percentage of coverage in Fig. 2-23) during the winter. Floating glacial ice, calved from glaciers, and winter bay ice is found in most of the bays and inlets from Annette, Alaska (Fig. 2-16), northward. A listing of calving tidewater glaciers in Alaska is given in Table 2-2 (Brower et al., 1988).

Figure 2-24 shows the Gulf of Alaska sea surface temperatures in August, which are about the warmest of the year. Again, the northward bulge of isotherms along the coast reflects the influence of the warm Alaska Current. Although Fig. 2-24 indicates "no ice of any kind reported in the area," this refers only to the open waters of the gulf. The bays and inlets of Alaska usually have bergs and growlers calved from glaciers at some locations throughout the year. Note that the Exxon Valdez ran aground while "dodging" Prince William Sound growlers (April 1989), resulting in an ecological disaster. Obviously bergs and growlers can be extremely hazardous to navigation.

to the western end of the Alaska Peninsula. The current is quite narrow with widths estimated from 2.7 to 13.5 n mi (5–25 km). Speed can be quite high reaching 2 to 3 kt (1–1.5 m/s) in some areas. Maximum speeds are usually noted in mid to late autumn.

Observations have shown that flow entering the Kennedy Entrance (between Barren Islands and Kenai Peninsula) to Cook Inlet is stronger and more persistent than flow entering the Stevenson Entrance (between Kodiak Island and Barren Islands). Speeds of 0.6 kt (0.3 m/s) are commonly observed, being stronger near the Kenai Peninsula. Superimposed on the current speed are tidal speeds reaching 1 kt (>0.5 m/s) in the Kennedy Entrance.

The current flow in Cook Inlet is interesting in that clear oceanic water enters the inlet from the southeast on the south side of the inlet during floodtide and departs as turbid water along the north and west coast during ebbtide. Currents near Kalgin Island, just east of the Redoubt Volcano (Fig. 2-18), are complex. In this region ebbtides and floodtides meet, speeds are higher, and occasional strong cross-inlet currents are observed. Peak velocities of 6 to 8 kt (3–4 m/s) occur during tidal extremes.

2.2.5 Tides

Figure 2-22 shows the range from high to low tide typical of the Gulf region. The tides are of the mixed type with two highs and two lows per day in most locations. It can be seen that a very high tidal range of 30 ft (9 m) is characteristic of the Anchorage area. Secondary maximum tides occur in Nushagak and Kvichak Bay at the northeast end of Bristol Bay.

2.2.6 Sea Ice and Sea Surface Temperature

February and March are typified by the coldest sea surface temperatures in the Gulf of Alaska. A bulging of the isotherms northward along the southeast coast of Alaska reflects the warming influence of the Alaska Current in that region. Figure 2-23 shows the mean sea surface temperature for February. The Gulf of Alaska is ice free throughout the year. However, Cook Inlet has appreciable ice amounts (shown as percentage of coverage in Fig. 2-23) during the winter. Floating glacial ice, calved from glaciers, and winter bay ice is found in most of the bays and inlets from Annette, Alaska (Fig. 2-16), northward. A listing of calving tidewater glaciers in Alaska is given in Table 2-2 (Brower et al., 1988).

Figure 2-24 shows the Gulf of Alaska sea surface temperatures in August, which are about the warmest of the year. Again, the northward bulge of isotherms along the coast reflects the influence of the warm Alaska Current. Although Fig. 2-24 indicates "no ice of any kind reported in the area," this refers only to the open waters of the gulf. The bays and inlets of Alaska usually have bergs and growlers calved from glaciers at some locations throughout the year. Note that the Exxon Valdez ran aground while "dodging" Prince William Sound growlers (April 1989), resulting in an ecological disaster. Obviously bergs and growlers can be extremely hazardous to navigation.

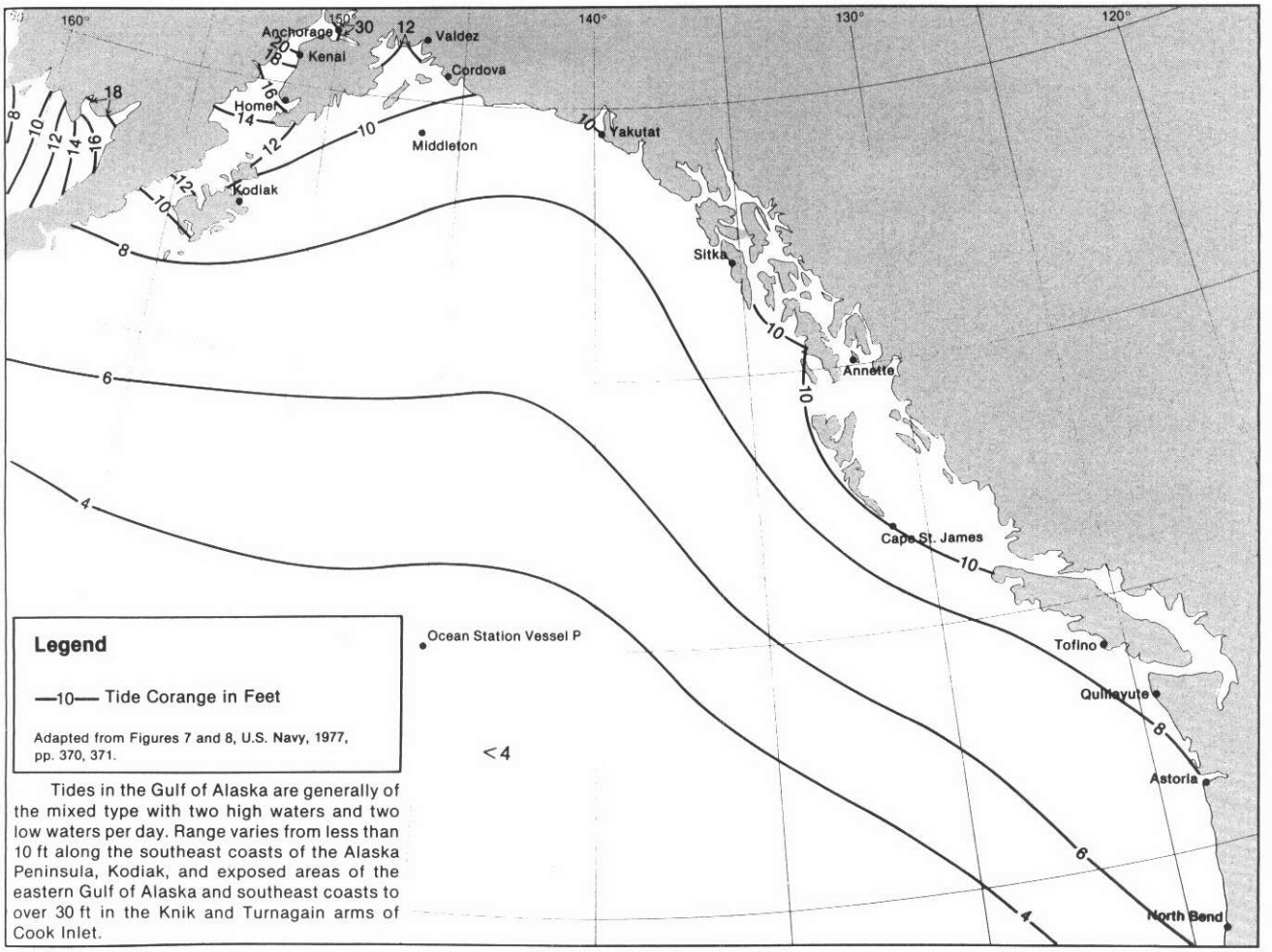

Figure 2-22. Gulf of Alaska tide corange (Brower et al., 1988).

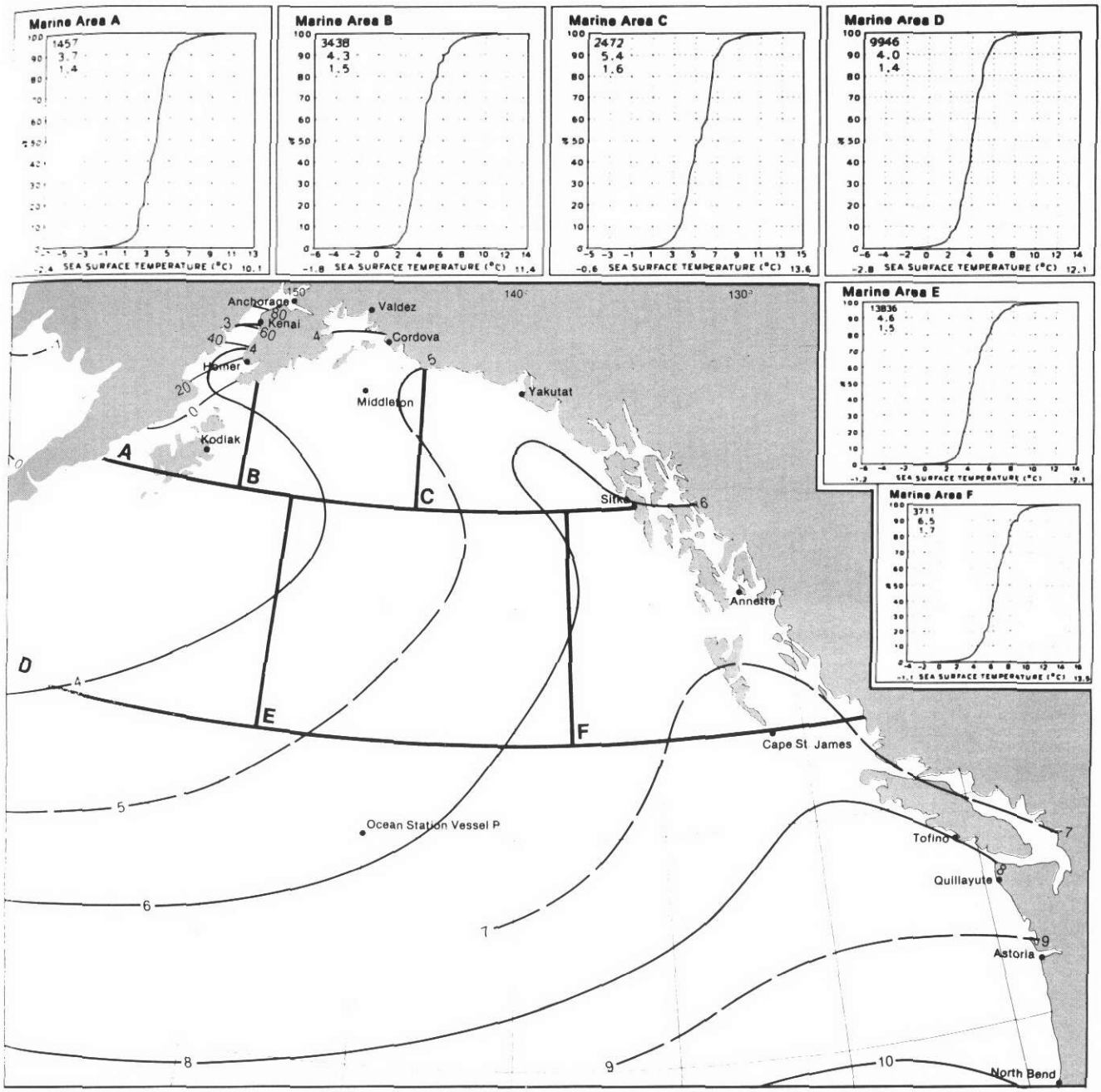

Figure 2-23. Gulf of Alaska mean sea surface temperature (°C) for February and ice of any kind (%) (Brower et al., 1988).

TABLE 2-2. CALVING TIDEWATER GLACIERS IN ALASKA, NUMBERED FROM SOUTH TO NORTH (BROWER ET AL., 1988)

Frederick Sound
1. Le Conte Glacier, in Le Conte Bay

Stevens Passage
2. Dawes Glacier, in Endicott Arm
3. South Sawyer Glacier, in Tracy Arm
4. Sawyer Glacier, in Tracy Arm
5. Taku Glacier, in Taku Inlet

Glacier Bay
6. McBride Glacier, in Muir Inlet
7. Riggs Glacier, in Muir Inlet
8. Muir Glacier, in Muir Inlet
9. Plateau Glacier, in Wachusett Inlet
10. Grand Pacific Glacier, in Tarr Inlet
11. Margerie Glacier, in Tarr Inlet
12. Toyatte Glacier, in Johns Hopkins Inlet
13. Johns Hopkins Glacier, in Johns Hopkins Inlet
14. Gilman Glacier, in Johns Hopkins Inlet
15. Hoonah Glacier, in Johns Hopkins Inlet
16. Kashoto Glacier, in Johns Hopkins Inlet
17. Lamplugh Glacier, in Johns Hopkins Inlet
18. Reid Glacier, in Reid Inlet

Cross Sound
19. Brady Glacier, in Taylor Bay

Northeast Gulf of Alaska
20. La Perouse Glacier

Lituya Bay
21. North Crillon Glacier
22. Cascade Glacier
23. Lituya Glacier

Yakutat Bay
24. East Nunatak Glacier, in Nunatak Fiord
25. Hubbard Glacier, in Disenchantment Bay
26. Turner Glacier, in Disenchantment Bay

Icy Bay
27. Tyndall Glacier
28. Yahtse Glacier
29. Guyot Glacier

Prince William Sound
30. Shoup Glacier, in Shoup Bay on Port Valdez
31. Columbia Glacier, in Columbia Bay
32. Meares Glacier, in Unakwik Inlet
33. Yale Glacier, in College Fiord on Port Wells
34. Harvard Glacier, in College Fiord on Port Wells
35. Smith Glacier, in College Fiord on Port Wells
36. Wellesley Glacier, in College Fiord on Port Wells
37. Coxe Glacier, in Barry Arm on Port Wells
38. Barry Glacier, in Barry Arm on Port Wells
39. Cascade Glacier, in Barry Arm on Port Wells
40. Serpentine Glacier, in Harriman Fiord on Port Wells
41. Surprise Glacier, in Harriman Fiord on Port Wells
42. Harriman Glacier, in Harriman Fiord on Port Wells
43. Blackstone Glacier, in Blackstone Bay
44. Beloit Glacier, in Blackstone Bay
45. Nellie Juan Glacier, in Derickson Bay on Port Nellie Juan
46. Chenega Glacier, in Nassau Fiord on Icy Bay
47. Tiger Glacier, in Icy Bay

Aialik Bay
48. Aialik Glacier
49. Holgate Glacier, in Holgate Arm

Harris Bay
50. Northwestern Glacier, in Northwestern Lagoon

Nuka Bay
51. McCarty Glacier, in McCarty Fiord
52. Dinglestadt Glacier (eastern tongue), in McCarty Fiord

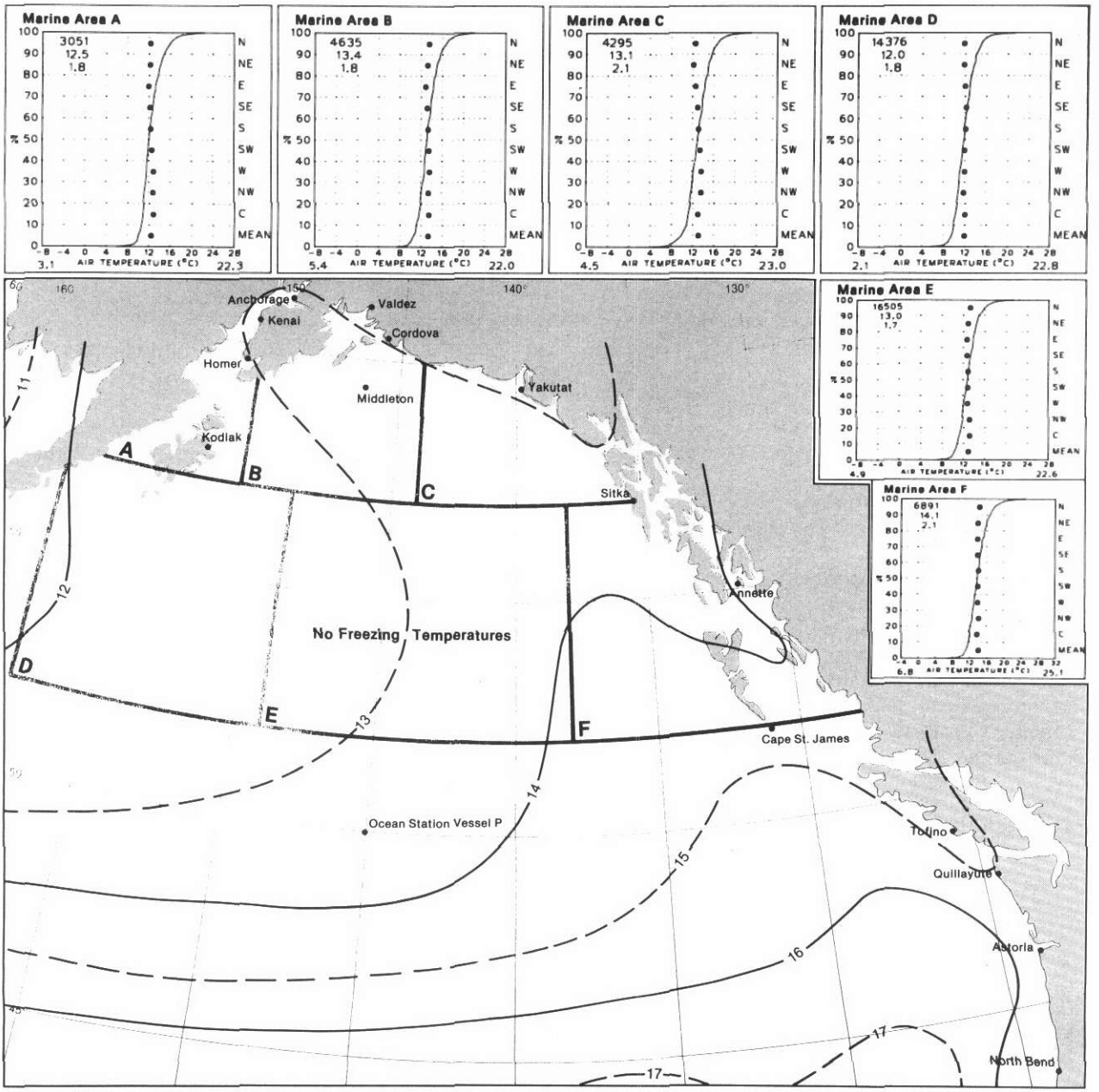

Figure 2-24. Gulf of Alaska mean sea surface temperature (°C) for August and ice of any kind (%) (Brower et al., 1988).